Weather and Climate Extremes 37 (2022) 100469

Contents lists available at ScienceDirect

Weather and Climate Extremes

journal homepage: www.elsevier.com/locate/wace

Combined role of ENSO and IOD on compound drought and heatwaves in Australia using two CMIP6 large ensembles

P. Jyoteeshkumar Reddy [a,b,*], Sarah E. Perkins-Kirkpatrick [a,b], Nina N. Ridder [b,c], Jason J. Sharples [a,b]

[a] School of Science, UNSW Canberra, ACT, Australia
[b] ARC Centre of Excellence for Climate Extremes, UNSW, Australia
[c] Climate Change Research Centre, UNSW, Sydney, NSW, Australia

ARTICLE INFO

Keywords:
Compound events
Drought
Heatwave
ENSO
IOD
SMILE

ABSTRACT

Compound drought and heatwaves (CDHWs) can cause significant socio-economic and ecological impacts. A better understanding of historical spatiotemporal changes of Australian CDHWs and their underlying physical mechanisms can help improve their predictability. We analyse changes in Australian CDHW metrics in the extended summer season (November to March) during the period 1958–2020. Our results suggest that CDHWs increased significantly in terms of their frequency, duration, amplitude, and severity in the recent period (1989/90–2019/20) relative to a historical period (1958/59–1988/89), particularly in eastern Australia. We further analysed the influence of co-occurring modes of El Niño Southern Oscillation (ENSO) and Indian Ocean Dipole (IOD) on the frequency and severity of Australian CDHWs using two Coupled Model Intercomparison Project phase 6 (CMIP6) single model initial-condition large ensembles. We found that frequency, duration, and severity of CDHWs are significantly increased during strong El Niño phases across northeast Australia compared to neutral ENSO and IOD conditions. This increase is widespread over northeast and southeast Australia during the concurrence of strong El Niños and moderate-strong positive IOD events. Our results show that an extreme CDHW season in terms of their frequency, duration, and severity occurs one out of every two seasons of strong El Niño over the northeast Australia. Moreover, the same applies for the co-occurring strong El Niño and positive IOD over the northeast and southeast Australia as well. Our results highlight the importance of ENSO and IOD combinations for Australian CDHW events. Our findings provide insights into the importance of climate variability in driving Australian CDHWs.

1. Introduction

Compound drought and heatwaves (CDHWs) are categorised as a multivariate type of compound event because the co-occurrence of two extreme events, i.e., drought and heatwave in the same location, cause massive impacts (Zscheischler et al., 2020). CDHW events have adverse effects on agricultural productivity (Ciais et al., 2005), human health (Fink et al., 2004), water resources (Coffel et al., 2019), biodiversity (Mo and Roache, 2021), and forest tree mortality (Allen et al., 2010). These events can result in considerable economic losses, e.g., the 2003 CDHW event in Europe resulted in 13.1 billion Euros losses to the forestry and agricultural industry (Fink et al., 2004). The combination of drought and heatwave events also have the potential to increase bushfire risk (Abram et al., 2021; Sharples et al., 2016), particularly through their effect on fine fuel moisture content (Reddy et al., 2021a). For instance, the compound influence of prolonged drought combined with repeated heatwaves during the 2019-20 summer provided conditions favourable for the unprecedented extent and devastating impacts that characterised the catastrophic Black Summer bushfires in Australia (Administration References Committee, 2019; Nolan et al., 2020).

CDHWs are defined as periods of heatwaves occurring during meteorological drought (Geirinhas et al., 2021; Mukherjee and Mishra, 2021; Wu et al., 2021). Heatwave definitions vary broadly among different groups based on the targeted sector-based applications (Perkins and Alexander, 2013). Heatwaves are generally defined as a continuous period of hot days with temperatures higher than a specific extreme threshold. The location-specific percentile thresholds used to define heatwaves account for regional climatic variations (Perkins and

* Corresponding author. School of Science, UNSW Canberra, ACT, Australia.
E-mail address: j.papari@student.adfa.edu.au (P.J. Reddy).

https://doi.org/10.1016/j.wace.2022.100469
Received 15 December 2021; Received in revised form 1 June 2022; Accepted 1 June 2022
Available online 4 June 2022

Alexander, 2013) and have been widely used in previous heatwave studies (Fischer and Schär, 2010; Perkins-Kirkpatrick and Lewis, 2020; Pezza et al., 2012).

Droughts are complex phenomena, defined in a multitude of ways based on targeted sector impacts and droughts are often classified as meteorological, hydrological, agricultural, or socio-economic droughts (Esfahanian et al., 2017). CDHWs generally consider drought as a meteorological drought, which is associated with rainfall deficits and are monitored using indices, such as the Standardised Precipitation Index (SPI) (Mckee et al., 1993), the Standardised Precipitation-Evapotranspiration Index (SPEI) (Vicente-Serrano et al., 2010) and the Palmer Drought Severity Index (PDSI) (Palmer, 1965). However, the SPI has been recommended by the World Meteorological Organisation (WMO) for monitoring meteorological drought (Hayes et al., 2011; WMO, 2012). Moreover, the temperature independence of the SPI makes it a favourable tool for the assessment of CDHW in the context of compound events (Geirinhas et al., 2021; Ionita et al., 2021; Kong et al., 2020; Mazdiyasni and AghaKouchak, 2015; Shi et al., 2021; Vogel et al., 2021).

Many previous studies have investigated changes in CDHWs across different parts of the world. For instance, Mazdiyasni and AghaKouchak (2015) analysed CDHWs over the United States during the historical period (1960–2010) and found a substantial increase in their frequency and spatial extent. Similar results have been found for Brazil (Geirinhas et al., 2021), China (Kong et al., 2020), Europe (Ionita et al., 2021), and India (Sharma and Mujumdar, 2017). Recently, Mukherjee and Mishra (2021) reported that CDHWs are becoming more frequent and intense in the recent period (2000–16) compared to the past (1983–99), particularly across the arid regions of Asia, Australia, Europe, and North America.

Australia has previously been identified as particularly prone to the occurrence of CDHWs (Ridder et al., 2020). Future projections indicate Australia will experience more frequent CDHWs under enhanced anthropogenic climate change (Ridder et al., 2022). These previous studies are limited to frequency analysis of CDHW events and can be extended by studying their multiple characteristics (like duration, amplitude, and severity), which is currently lacking. Little is known about the characteristics of CDHW events in Australia. It is important to analyse the multiple characteristics of CDHWs, because of their potential for significant socio-economic and ecological impacts across a wide range of sectors. In view of Australia's proneness to CDHWs, understanding the response of CDHW characteristics to the already experienced warming over the past decades is therefore crucial.

In many regions across the globe, including Australia, favourable environments for the development of heatwaves and meteorological droughts are created by atmospheric processes driven by large-scale modes of climate variability (Hao et al., 2018; Loughran et al., 2019; Mukherjee et al., 2020; Perkins et al., 2015; Ummenhofer et al., 2009). For example, Hao et al. (2018) found that El Niño Southern Oscillation (ENSO (Trenberth, 1997)) had a significant influence on compound dry and hot events in Australia, southeast Asia, and southern Africa. Similarly, Mukherjee et al. (2020) found that ENSO had a substantial impact on the frequency and severity of austral summer CDHWs over Australia, southern Africa, and the Amazon basin. Indeed, ENSO and the Indian Ocean Dipole (IOD (Saji et al., 1999)) are the climate modes that influence the occurrence of heatwaves (Perkins et al., 2015) and droughts (Meyers et al., 2007; Ummenhofer et al., 2011) across eastern and southeastern Australia. The combined effect of these climate modes on drought and heatwaves in Australia has been previously studied for each of the two extremes in isolation (Reddy et al., 2021c; Ummenhofer et al., 2011). Ummenhofer et al. (2011) found that cool season (June–October) drought conditions over southeast Australia are associated with co-occurring phases of El Niño and positive IOD. Reddy et al. (2021c) found that extended summer season (November–March) contiguous heatwaves over Australia cover larger areas with increased intensity during strong El Niño and its concurrence with strong positive IOD compared to the neutral phase of both ENSO and IOD. Based on the previous studies (Reddy et al., 2021c; Ummenhofer et al., 2011), it can be hypothesised that the combination of El Niño and the positive IOD phase might be linked with CDHW conditions over Australia during the extended summer season. However, the influence of co-occurring ENSO and IOD phases on extended summer season CDHWs in Australia has not yet been researched.

Here, we quantify the observed spatiotemporal changes of CDHW characteristics during the recent period 1989/90–2019/20 compared to the historical period 1958/59–1988/89 in Australia. Further, we use the single model initial-condition large ensemble (SMILE) of the Coupled Model Intercomparison Project phase 6 (CMIP6) models to specify the effects of natural variability on CDHWs. A SMILE is a suite of model simulations produced with a single climate model by varying initial conditions and with same external forcing. Each member in SMILE is applied with different initial conditions, which creates diverging climate trajectories (Maher et al., 2021). A SMILE provides a large sample of extreme events under many different climate conditions, which allows us to statistically quantify the role of climate variability on extreme events (Schaller et al., 2018). SMILE has been widely used to analyse the effects of climate variability on extreme events and has been identified as a reliable tool for this type of assessment (Reddy et al., 2021c). Our analysis quantifies the effects of recent observed warming on CDHWs in Australia and will help to improve our understanding of the climate drivers of Australian CDHWs.

2. Data and methods

2.1. Data

We used monthly rainfall and daily maximum and minimum temperature of the Australian Gridded Climate Data (AGCD)/Australian Water Availability Project (AWAP) gridded dataset covering the Australian continent for the period from 1910 to 2020 (Jones et al., 2009). It is constructed by applying the complex gridding procedure on Australia's available quality-controlled station data (Jones et al., 2009). We performed our analysis using the $0.25^\circ \times 0.25^\circ$ resolution data instead of $0.05^\circ \times 0.05^\circ$ fine resolution data to comply with computational limitations. Previous studies have suggested that this reduction in grid resolution did not influence the magnitude and spatial trend pattern of heatwaves (Perkins and Alexander, 2013). The AGCD/AWAP dataset has been extensively used for studying droughts (Gallant et al., 2013) and heatwaves (Herold et al., 2016; Reddy et al., 2021b; Perkins et al., 2015) in Australia. To ensure optimal data coverage with a dense station network, which for AGCD/AWAP was realised in 1957 (Herold et al., 2016; Jones et al., 2009), we only use data from 1958 to 2020, i.e., November 1958 to March 2020. We have masked the regions of less dense station network with no nearest station ($<2^\circ$ radius) containing at least 90% of non-missing monthly rainfall data during the period 1958–2020. The station locations are extracted from the AGCD/AWAP station network.

Monthly sea surface temperature (SST) observations for the identification of climate modes, i.e., ENSO and IOD indices, over the same time period is obtained from the Hadley Centre Global Sea Ice and Sea Surface Temperature (HadISST v1.1) dataset (Rayner et al., 2003). This dataset provides a small sample of co-occurring phases of ENSO and IOD (Reddy et al., 2021c). Hence, we complemented the HadISST dataset with monthly SST, daily maximum and minimum temperature, monthly rainfall, and monthly sensible and latent heat fluxes data from the CMIP6 SMILEs (CNRM-CM6-1 and CanESM5) historical experiment for the period 1958–2014. A SMILE provides a larger sample of the seasons of different co-occurring modes of ENSO and IOD compared to observations, which allows for robust quantification of their influence on extreme events (Reddy et al., 2021c). We use the SMILEs instead of a multi-model ensemble with a single or a few members from each model for two reasons. One is that SMILE provides a large sample of extreme

events under many different climate conditions, which a multi-model ensemble cannot. The other is that the multi-model ensemble contains the mixture of structural uncertainty (i.e., model-specific uncertainties) and uncertainty from internal variability, where SMILE can address both separately (Maher et al., 2021; Wood et al., 2021).

We used the data from the CNRM-CM6-1 SMILE (r(1–30)i1p1f2) (Voldoire et al., 2019) but excluded the r2i1p1f2 and r25i1p1f2 members data because of previously defined large errors in heatwave calculation (Reddy et al., 2021c). The CNRM-CM6-1 SMILE reproduced observed climatology and probability distributions of extreme Australian temperatures well compared to other CMIP6 SMILEs during the historical period (1950–2014) (Deng et al., 2021). However, previous studies showed that the estimates of climate variability differ among various SMILEs (Deng et al., 2021; Lehner et al., 2020; Maher et al., 2020). Hence, in addition to CNRM-CM6-1, we used the CanESM5 SMILE (Swart et al., 2019) r(1–25)i1p1f1 data to perform the complete analysis, which increases the confidence of our results. We have used the CanESM5 SMILE because Deng et al. (2021) showed that next to CNRM-CM6-1, CanESM5 SMILE reasonably represented the distributions and climatology of extreme temperatures in Australia.

2.2. Defining compound drought and heatwaves (CDHWs)

2.2.1. Heatwave definition

We use the definition of heatwaves introduced by Perkins and Alexander (2013) based on the excess heat factor (EHF) (Nairn and Fawcett, 2013). As such, we define a heatwave as a period of three or more successive days with an EHF value greater than zero. A heatwave is considered continued until two consecutive days have zero or below zero EHF values (Reddy et al., 2021c). This definition overcomes the limitation of consecutive day criteria by allowing a break of a normal or non-heatwave day and enables us to estimate the actual length of the heatwave containing minor breaks of normal or non-heatwave days in its duration (Baldwin et al., 2019; Rastogi et al., 2020). This definition has been proven useful and has been widely used in previous studies (Baldwin et al., 2019; Rastogi et al., 2020). We calculate EHF according to Reddy et al. (2021b) as follows:

$$T = \frac{(T_{max} + T_{min})}{2} \tag{1}$$

$$EHI_{sig} = \frac{(T_i + T_{i-1} + T_{i-2})}{3} - T_{90} \tag{2}$$

$$EHI_{acc} = \frac{(T_i + T_{i-1} + T_{i-2})}{3} - \frac{(T_{i-3} + \ldots + T_{i-32})}{30} \tag{3}$$

$$EHF = EHI_{sig} \times max(EHI_{acc}\ ,\ 1) \tag{4}$$

where T_{max} and T_{min} are the daily maximum and minimum near-surface air temperatures, respectively. T_i is the daily mean temperature on the ith day and T_{90} is the climatological 90th percentile temperature of this day relative to a selected base period (here 1961–90). The same base period is considered for both the observations and model data. EHI_{sig} and EHI_{acc} are the significance and the acclimatisation excess heat indices, respectively.

2.2.2. Drought definition

We define drought at a monthly timescale using the Standardised Precipitation Index (SPI (Mckee et al., 1993);). SPI is based on cumulative precipitation time series that are fitted to a gamma distribution, with the SPI being the number of standard deviations the cumulative precipitation deviates from the climatological mean (Mckee et al., 1993). As such, the SPI is independent of temperature, which makes it a widely used drought metric for the investigation of the compound nature of CDHW events (Geirinhas et al., 2021; Ionita et al., 2021; Kong et al., 2020; Mazdiyasni and AghaKouchak, 2015; Vogel et al., 2021).

SPI can be calculated at various monthly timescales (e.g., 3-, 6-, 9-, 12-, 24- and 48-month scales), signifying the length of time over which accumulated precipitation is calculated (Mckee et al., 1993). The shorter timescale (e.g., 3-month) SPI represents soil moisture conditions, whereas long timescales (12-, 24- and 48-month) indicate groundwater and water storage levels (i.e., hydrological drought conditions) (Guenang and Mkankam Kamga, 2014; Spinoni et al., 2014; Vogel et al., 2021; WMO, 2012). We considered a meteorological drought to occur in each month with an associated 3-month SPI (SPI-3) value below or equal to two thresholds, namely −0.5 (mild drought) and −1 (moderate drought). Many previous studies have also considered SPI-3 ≤ -0.5 or ≤ -1 as drought thresholds in defining CDHWs (Geirinhas et al., 2021; Ionita et al., 2021; Wu et al., 2021). While these SPI thresholds indicate relatively mild drought conditions, the compounding effect together with extreme heat, can still cause severe impacts as commonly seen during compound events (Seneviratne et al., 2012).

2.2.3. Definition of compounding dry and heatwave events

A CDHW event is defined as the period of a heatwave that commenced during a month of drought. This CDHW definition considers the ongoing effects of drought on the development of heatwaves and accommodates the different timescales of both extremes. It has been effectively applied to other regions in recent studies (Shi et al., 2021). According to this definition, heatwaves that started during a month of no drought conditions and extended into a month of drought are not considered as CDHWs and instead identified as only heatwave events (Shi et al., 2021).

2.3. CDHW metrics

CDHW events can be characterised using various metrics, including frequency, duration, severity (Mukherjee and Mishra, 2021), and amplitude (Table 1).

We analyse these CDHW metrics for the extended summer season (NDJFM) during the period 1958–2020 using the AWAP data across Australia. We split this period into two separate periods, 1958/59–1988/89 (past period) and 1989/90–2019/20 (current period) and assess changes in the different CDHW metrics (not detrended). The statistical significance of changes of CDHW metrics between these two periods is assessed with the non-parametric permutation test. The permutation test is distribution independent and can be used to test the significance of non-normally distributed CDHW metrics data (DelSole et al., 2017; Singh et al., 2021). We considered the significance level as 0.05 and set the permutations to 10,000 times (further information is provided in Sec. 2.6) (Singh et al., 2021).

2.4. Evaluation of CNRM-CM6-1 and CanESM5 SMILEs

To evaluate the CNRM-CM6-1 and CanESM5 SMILE's ability in simulating the CDHWs over Australia, we compared the ensemble mean

Table 1
Definition of CDHW metrics and their abbreviations used in this study.

CDHW metric	Abbreviation	Description	Units
Frequency	CDHWF	Total number of CDHW days in a season	Days/season
Duration	CDHWD	Duration of the longest CDHW event in a season	Days/season
Daily magnitude of CDHW $= (-2 \cdot SPI_j) \cdot EHF_i$ $i = day; j = corresponding\ month$			$^{\circ}C^2$
Amplitude	CDHWA	Maximum magnitude reached by the intense CDHW event on a particular day in a season.	$^{\circ}C^2$/season
Severity	CDHWS	The seasonal sum of magnitude across all CDHW days	$^{\circ}C^2$/season

of CDHW metrics in SMILEs with the observational gridded data during the period 1958/59–2013/14. For the comparison, we calculated the model's bias in simulating CDHWs as the difference between the ensemble mean of SMILE's and the re-gridded observations. The observational data is re-gridded to the respective model's resolution (CNRM-CM6-1 - 1.4008° × 1.40625° and CanESM5 - 2.7906° × 2.8125°) using the bilinear interpolation technique. Further, we evaluate each SMILE's ability in capturing the observed variability in CDHWs over Australia during the period 1958/59–2013/14 by considering the evaluation framework followed by Maher et al. (2019), Reddy et al. (2021c), Suarez-Gutierrez et al. (2020), and Wood et al. (2021). In this framework, the observed anomalies of CDHW metrics are compared with the anomalies of each SMILE member. The anomalies are calculated with respect to the selected reference period 1961–90. By following this method, we considered each SMILE to be underestimating the observed variability if more than 15% of observed anomalies fall outside the whole ensemble range (0 - 100th percentile) (Fig. 1 (a)). A SMILE is considered as overestimating the observed variability only if more than 85% of observed anomalies lie inside the central 75th percentile range (12.5th - 87.5th percentile) of the ensemble and less than or equal to 15% observed anomalies lie inside the ensemble range (Fig. 1 (b)). Each SMILE is considered to be exhibiting a satisfactory bias with the observations in representing the variability when more than or equal to 85% of observed anomalies are within the ensemble range (not underestimating variability) and less than or equal to 85% in the central 75th percentile range of the ensemble (not overestimating variability) (Fig. 1 (c)).

2.5. ENSO and IOD

We linearly detrend the SST data used to calculate the ENSO and IOD indices to remove the global warming signal. We quantified ENSO using the Niño3.4 index (Trenberth, 1997), which is calculated as the average of SST anomalies (relative to the period 1961–90) over the region

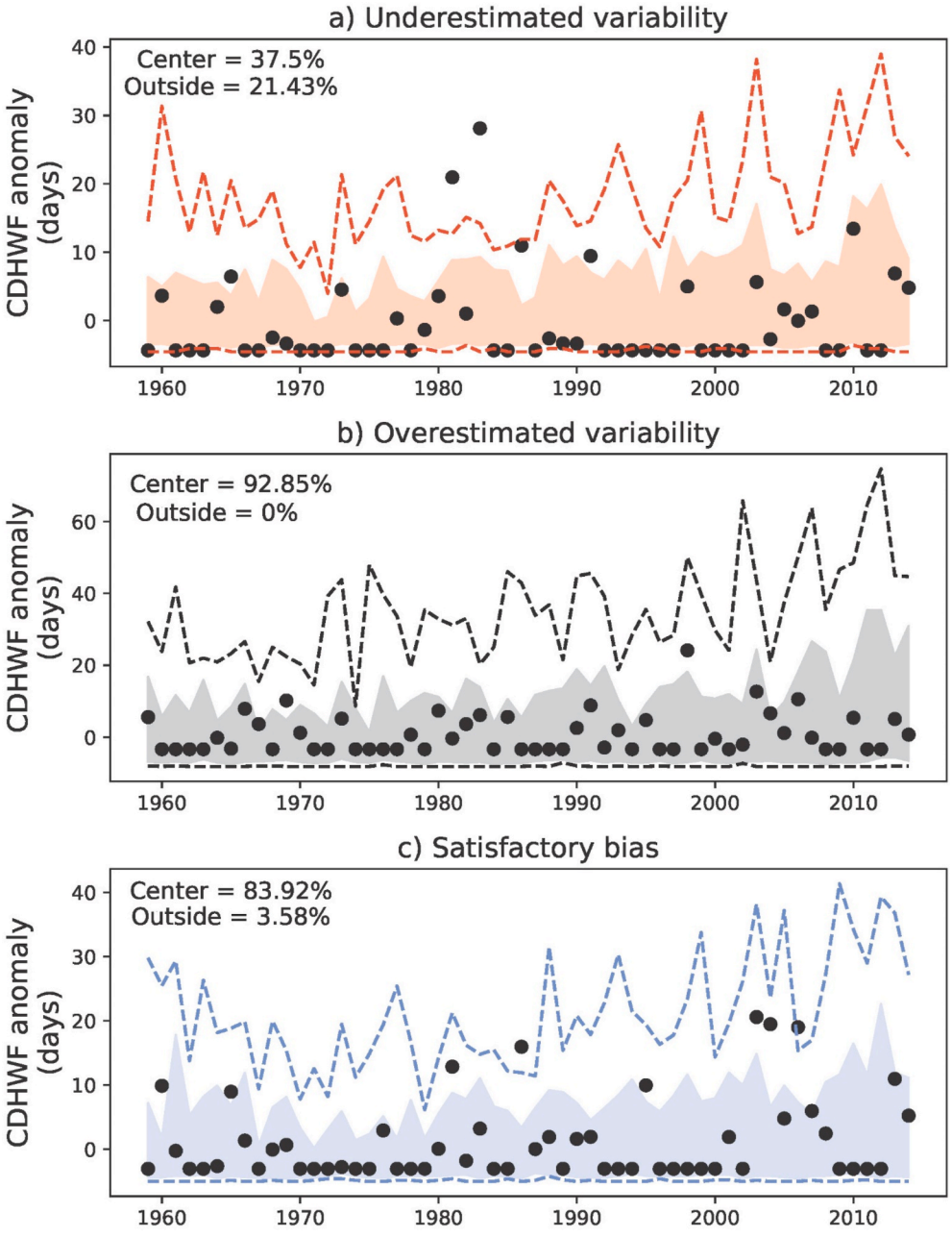

Fig. 1. An example of time series of CDHWF anomalies relative to 1961-90 using CNRM-CM6-1 SMILE (colour shading and dotted lines) and observations (black dots). Colour shading represents the central 75th percentile range (12.5th - 87.5th percentile), and dotted colour lines represent ensemble minimum and maximum. Black dots represent observed anomalies. The center percentage values represent the percent of observations within the central 75th percentile range, and outside percentage values represent the percent of observations outside the ensemble range. (For interpretation of the references to colour in this figure legend, the reader is referred to the Web version of this article.)

5°N–5°S, 170°W–120°W. ENSO strength is highly correlated with heatwave characteristics over Australia (Perkins et al., 2015). Hence, to include the influence of ENSO strength variations on Australian CDHWs, we categorised ENSO according to Casselman et al. (2021) and Reddy et al. (2021c) into moderate and strong events, expressed in equation (5).

$$ENSO\ phase = \begin{cases} strong\ El\ Niño\ ,\ Niño3.4 > 1\sigma \\ moderate\ El\ Niño\ ,\ 0.5\sigma < Niño3.4 \leq 1\sigma \\ \quad neutral\ ,\quad -0.5\sigma \leq Niño3.4 \leq 0.5\sigma \\ moderate\ La\ Niña\ ,\ -0.5\sigma > Niño3.4 \geq -1\sigma \\ strong\ La\ Niña\ ,\ Niño3.4 < -1\sigma \end{cases} \quad (5)$$

We use the dipole mode index (DMI) as a measure for the IOD (Saji et al., 1999). The DMI is calculated as the difference in SST anomalies (relative to 1961–90) between the west tropical Indian Ocean (50°E–70°E, 10°S–10°N), and southeast tropical Indian Ocean (90°E–110°E, 10°S–0°N). Like ENSO, we categorised the IOD as moderate and strong events to accommodate the variations of IOD's strength in our study (see eq. (6)).

$$IOD\ phase = \begin{cases} strong\ IOD\ positive\ ,\ DMI > 1\sigma \\ moderate\ IOD\ positive\ ,\ 0.5\sigma < DMI \leq 1\sigma \\ \quad neutral\ ,\ -0.5\sigma \leq DMI \leq 0.5\sigma \\ moderate\ IOD\ negative\ ,\ -0.5\sigma > DMI \geq -1\sigma \\ strong\ IOD\ negative\ ,\ DMI < -1\sigma \end{cases} \quad (6)$$

We combined the co-occurrences of ENSO and IOD using their respective classified phases (see eqs. (5) and (6)), which resulted in a total of 25 phase groups (5 × 5) (see Table 2). For example, a moderate El Niño season is defined as a season with ENSO in the moderate El Niño phase ($-0.5\sigma \leq Niño3.4 \leq 0.5\sigma$) and IOD in the neutral phase ($-0.5\sigma \leq DMI \leq 0.5\sigma$). A detailed list of all possible combinations is presented in Table 2.

2.6. Approach

To study the combined role of ENSO and IOD on CDHWs, the composite mean difference of CDHW metrics is calculated between the co-occurring phases of ENSO and IOD and the neutral ENSO and neutral IOD conditions. The significance of the composite mean difference is assessed using the non-parametric permutation test (Good, 2013). The permutation test can be applied to both continuous and categorical data (Good, 2013). The permutation test has been widely used to test the statistical significance of composite analysis (Reddy et al., 2021c; Singh et al., 2021, 2022). In this test, the first step is to calculate the difference in the means of two original distributions (for example p and q of sizes x and y, respectively). The second step is to randomly generate the two new distributions (of sizes x and y, respectively) from the combined permuted sample of the two original distributions (p and q) and recalculate the difference in the means of these distributions. The third step is to reiterate the second step for 10,000 times to get a distribution of the mean difference values. If the difference in the means of two original distributions is higher (lower) than the 95th (5th) percentile of the randomly generated distribution of the mean difference values, then that is considered as significantly different.

We use the evaporative fraction (*EF*) to assess the land surface conditions during the combinations of ENSO and IOD phases. EF represents the division of available energy between sensible and latent heat. EF is used as a proxy for soil moisture, with low EF values indicating dry conditions and high EF values indicating moist conditions (Donat et al., 2017). However, daily net radiation and meteorological conditions can regulate the soil moisture - EF relationship (Ford et al., 2014). EF is calculated using the US National Oceanic and Atmospheric Administration (NOAA) - Cooperative Institute for Research in Environmental Sciences (CIRES) Twentieth Century Reanalysis (20CR) version 2c data (Compo et al., 2011), CNRM-CM6-1 and CanESM5 SMILEs data as follows:

$$EF = \frac{Q_e}{Q_e + Q_h} \quad (7)$$

where Q_e and Q_h are the monthly latent and sensible heat fluxes. *EF* values beyond 0–1 range are not considered for the analysis. The average extended summer *EF* values are used to calculate the composite differences between combinations of ENSO and IOD phases and the neutral phase.

Table 2
Total 25 co-occurring phases of ENSO and IOD and the number of their occurrence in observations (1958–2020), CNRM-CM6-1 and CanESM5 SMILEs (1958–2014) (Reddy et al., 2021c). Note that the event numbers for both climate models are totals over all ensemble members. The data is shown as follows 'observations {CNRM-CM6-1} [CanESM5]'. The total number of extended summers examined for the observations, CNRM-CM6-1, and CanESM5 SMILEs are 63, 1596, and 1425.

Phase:- ENSO→ IOD ↓	Strong La Niña	Moderate La Niña	Neutral	Moderate El Niño	Strong El Niño
Strong IOD negative	2 {118} [28]	2 {84} [19]	4 {103} [60]	0 {16} [15]	0 {5} [7]
Moderate IOD negative	4 {41} [34]	1 {36} [35]	4 {67} [110]	1 {23} [36]	0 {8} [38]
Neutral	2 {64} [76]	6 {50} [84]	9 {169} [241]	6 {83} [118]	3 {61} [114]
Moderate IOD positive	1 {28} [16]	1 {29} [19]	2 {127} [50]	1 {76} [33]	1 {120} [59]
Strong IOD positive	0 {6} [19]	1 {13} [23]	1 {85} [84]	4 {59} [22]	6 {97} [60]

3. Results

3.1. Observed changes in CDHWs across Australia

The changes of CDHW metrics during the recent period (1989/90–2019/20) compared to the past period (1958/59–1988/89) over Australia were calculated for both drought thresholds (i.e., SPI-3 ≤ −0.5 and SPI-3 ≤ −1) and are presented in Fig. 2. Both thresholds show a similar spatial pattern of significant changes in CDHW metrics. However, CDHW using the lower drought threshold (SPI-3 ≤ −0.5) show more widespread positive changes in the CDHW metrics than the CDHWs using the stricter threshold of moderate drought (SPI-3 ≤ −1). Overall, the results show that all four CDHW metrics considered here have increased in the recent period compared to the past, particularly in east Australia (Fig. 2). For example, CDHW frequency (CDHWF) has largely increased by 3–5 days/season under warmer climate conditions (Fig. 2 (a and e)). Large statistically significant changes can be found in the east and, for CDHWs with SPI-3 ≤ −0.5, the central west of the country. However, we are not confident about the changes in the central west region given the proximity of masked regions with low station density. Similar statistically significant changes are produced for event duration with changes of 1.5–2.5 days/season (Fig. 2 (b and f)). Neither of the two metrics of CDHW using the lower drought threshold shows a decrease under recent conditions, particularly in eastern Australia. In contrast, CDHW amplitude and severity show several regions with non-significant decreases, closer to the central east of the continent. The statistically significant changes are located in the east of Australia and show increases of 10–12 °C^2/season for amplitude, and 75–85 °C^2/season for severity (Fig. 2 (e–h)). At the same time, these fall within the same regions as the increases in frequency and duration. This suggests that the regions that experienced more frequent occurrences of CDHWs in the recent period compared to the past also experienced an increase in prolonged and severe CDHWs.

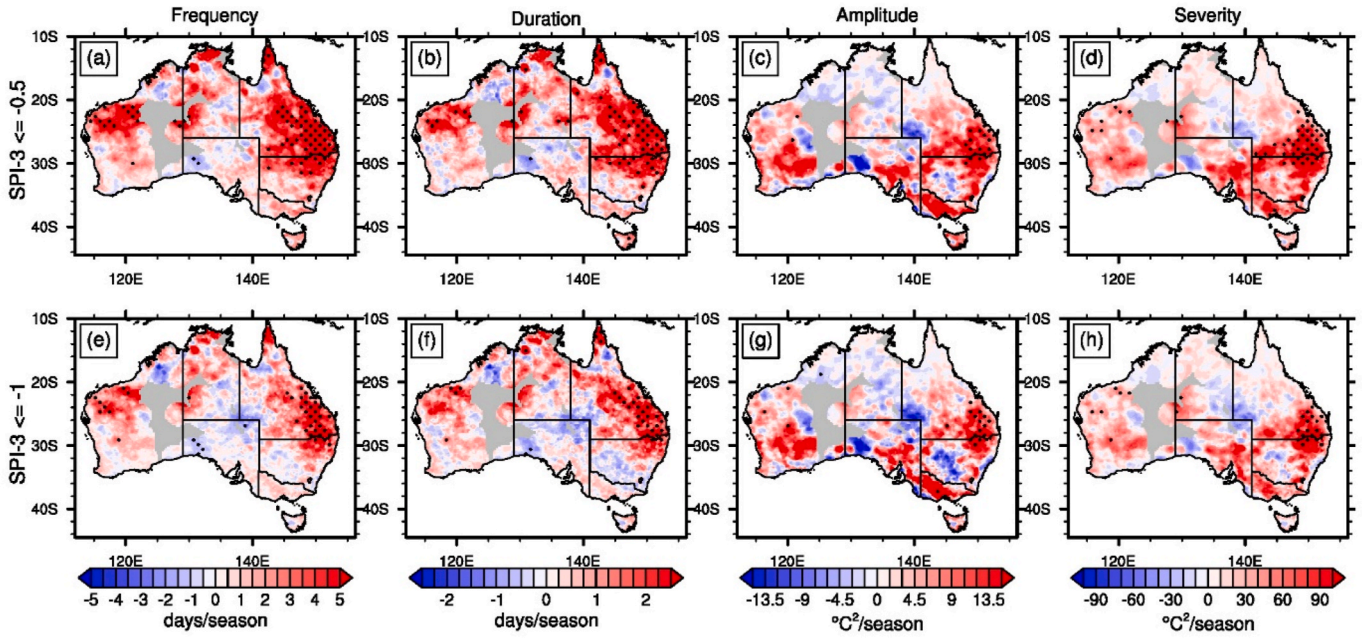

Fig. 2. Change in observed CDHW metrics (CDHWF (a and e), CDHWD (b and f), CDHWA (c and g), and CDHWS (d and h)) as realised in the AWAP dataset during the recent period (1989/90–2019/20) compared to the past period (1958/59–1988/89). Drought is defined using SPI-3 ≤ -0.5 (a–d) and SPI-3 ≤ -1 (e–h). The stippled regions represent the difference at the 0.05 significance level. Grey areas represent the masked regions. Regions of less dense station network are masked (refer to Sec.2.1).

3.2. Evaluating CDHWs mean and variability in the CNRM-CM6-1 and CanESM5 SMILEs

The evaluation of CNRM-CM6-1's skill in simulating observed CDHW metrics and their estimated variability over Australia is presented in Fig. 3. In general, CNRM-CM6-1 is able to capture the observed spatial patterns of the CDHW metrics over Australia reasonably well (see in Fig. 3 (a–h)). However, CNRM-CM6-1 shows a positive bias in all metrics across Australia's northern and eastern regions (Fig. 3 (a–h)). We also find that more than 85% of observed anomalies of CDHWF and CDHWD (CDHWA and CDHWS) clustered inside the 75th percentile range of CNRM-CM6-1 over the eastern and southwestern (eastern and northern) regions of Australia, indicating that simulated variability of respective CDHW metrics is slightly overestimated in those regions (see in Fig. 3 (i–l)). However, results also show that observations occur within the ensemble spread over most of the regions in Australia except central and southern parts (see in Fig. 3 (i–l)). In central and southern Australian regions, particularly CDHWA and CDHWS observed anomalies are outside the ensemble spread for more than 15% of the time (see in Fig. 3 (k and l)). This highlights that CNRM-CM6-1 may underestimate the variability in CDHWA and CDHWS over those regions. Overall, the evaluation of CNRM-CM6-1 suggests that the model simulated the observed CDHWs variability adequately over most regions of Australia. These results are consistent over the two different CDHW drought thresholds (not shown).

The same analysis for CanESM5 reveals similar biases as the CNRM ensemble (Supplementary Fig. S1). However, the positive biases in CanESM5 for all CDHW metrics are greater in magnitude and more widespread than those in CNRM-CM6-1 (Supplementary fig. S1 (a-h)). Further, CanESM5 overestimates the variability of all CDHW metrics compared to observations over most parts of Australia (Supplementary fig. S1 (i-l)). Overall, the substantial positive biases of all CDHW metrics and the overestimation of their variability by CanESM5 highlights the risk of overestimating CDHW metrics response to both external forcing and internal variability across Australia. This suggests the risk of overestimation of the magnitude of CDHW composites over Australia using the CanESM5 model.

3.3. The combined influence of ENSO and IOD on CDHWs in Australia

3.3.1. Composite differences in CDHW metrics

We use composites to investigate the combined influence of ENSO and IOD on Australian CDHWs. The composite differences of CDHW metrics (Table 1) during the respective co-occurring phases of ENSO and IOD relative to the neutral phase are computed. Detrending the CDHW metrics had a minimal effect on the results. For the purposes of this study, we only show the results obtained without removing the trend from CDHW metrics data. We only present results for CDHWs with a drought threshold of SPI-3 ≤ -0.5 as modelled by the CNRM-CM6-1 (Figs. 4 and 5) and CanESM5 (Supplementary Figs. S2–S3) SMILEs. Results for CDHWs using SPI-3 ≤ -1 are similar to these results with slightly lower values but the same spatial patterns (not shown). We have not shown the results of El Niño with IOD negative and La Niña with IOD positive combinations because these phases have occurred only a few instances in both SMILEs and very rarely in the observed period (Table 2).

The total number of CDHW days in a season (CDHWF) is largely influenced by ENSO with the lower CDHWF values during strong La Niña phases and higher during the strong El Niño phases in both SMILEs (CNRM-CM6-1 and CanESM5) compared to the neutral phase (compare the Fig. 4 (g) with 4 (k) and Supplementary Fig. S2 (g) with S2 (k), respectively). In contrast, CNRM-CM6-1 results show that the IOD is exhibiting a negligible impact with no statistically significant anomalies in CDHWF during both the positive and negative phases of the IOD (notice the lack of shading in Fig. 4 (c and o)). However, CanESM5 suggests that the IOD has a moderate effect on CDHWF with an overall increase during the positive phase of IOD, while the negative phase induces weak negative CDHWF anomalies (Supplementary Fig. S2 (c and o)). CanESM5 shows greater composite differences of CDHWF than CNRM-CM6-1 during co-occurring phases of El Niño and IOD positive. This might be due to the overestimation of CDHW metrics and their variability by CanESM5.

Overall, statistically significant positive anomalies in CDHWF are seen during the strong El Niño phase in isolation and also its co-occurrence with positive IOD phases (moderate and strong) over

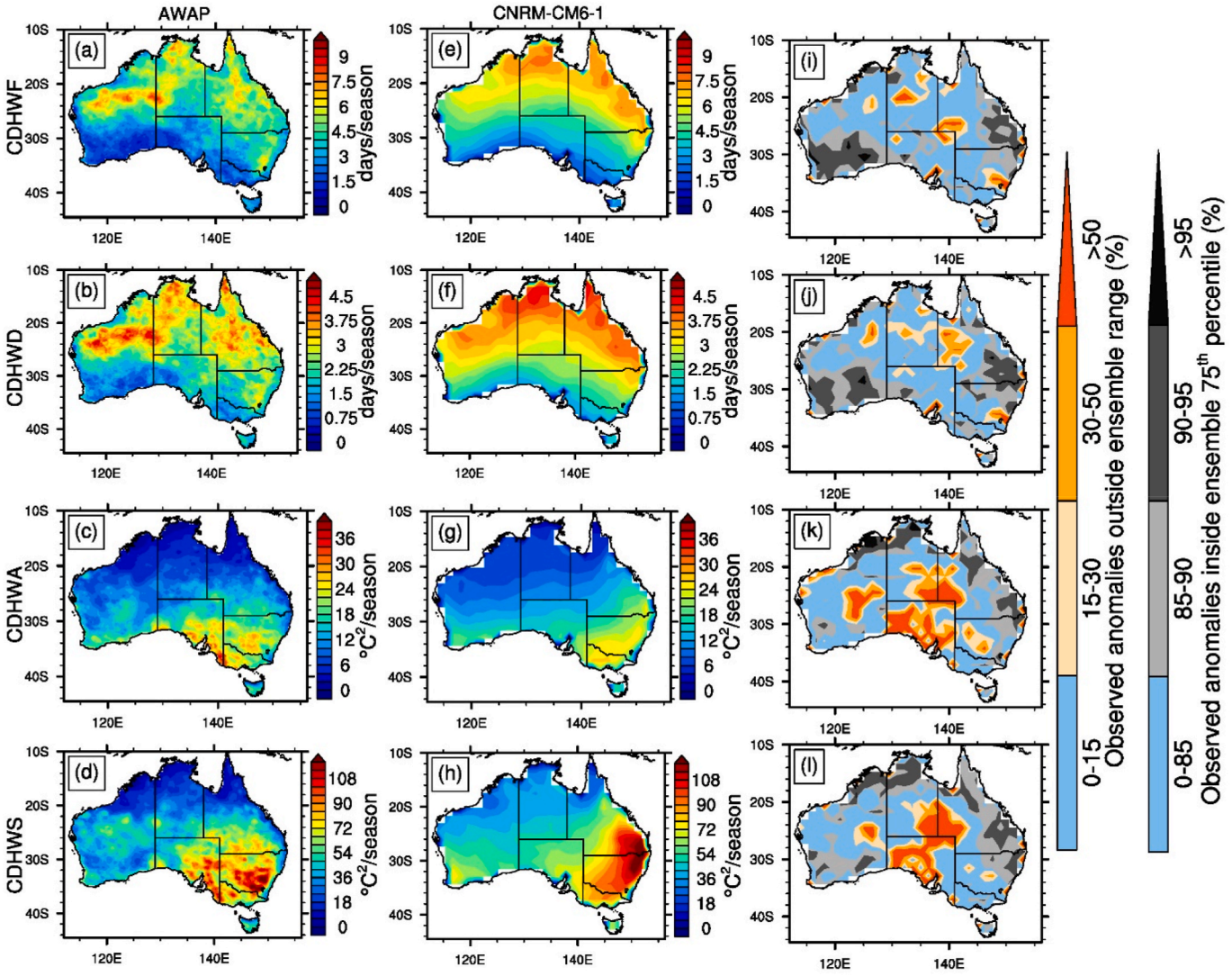

Fig. 3. Climatology of considered CDHW metrics using the AWAP data (a–d), the CNRM-CM6-1 SMILE ensemble mean (e–h) based on the period 1958/59–2013/14. CNRM-CM6-1 model grid points with at least 10% land area fraction are only shown (e–l). The evaluation of CDHW metrics variability simulated by the CNRM-CM6-1 SMILE (see section 2.4 for information on evaluation method; i-l). Grey to dark grey shading shows areas with overestimating simulated variability, and orange to red shading represents underestimating variability (i–l). Sky blue shading regions show satisfactory bias (with less than 15% of observed anomalies outside the ensemble range and less than 85% in the central 75th percentile range of the ensemble) in simulating the CDHW metrics variability (i–l). The drought threshold is considered as SPI-3 ≤ -0.5 in defining CDHWs. (For interpretation of the references to colour in this figure legend, the reader is referred to the Web version of this article.)

Australia compared to the neutral phase in both SMILEs (CNRM-CM6-1 and CanESM5) (see Fig. 4 (k, n, and q) and Supplementary Fig. S2 (k, n, and q)). This highlights the dominance of ENSO on changes in CDHWF. Moreover, CNRM-CM6-1 shows that the average increases in CDHWF are highest (of about six days/season compared to neutral conditions) during the strong El Niño phase over northern and northeast Australia (Fig. 4 (k)). However, more widespread increases (compared to the neutral conditions) are seen across northern, southern, and eastern Australia during the concurrence of strong El Niño with positive IOD phases than strong El Niño alone (Fig. 4 (n) and (q)). In contrast, CanESM5 results suggest that both the highest (of about eight days/season compared to neutral conditions) and more widespread increases in CDHWF over much of Australia are seen during the concurrent strong El Niño and strong positive IOD phase (Supplementary Fig. S2). Strong La Niña produce comparable negative anomalies in both the SMILEs, while these anomalies are seen over much of Australia in CanESM5 and are only limited to the northwest, northern subtropical and tropical regions of Australia in CNRM-CM6-1.

Similar results are found for the CDHW duration (not shown). Again, strong La Niña generates negative anomalies compared to neutral, while strong El Niño and its associated positive IOD phases cause increases (of about three days/season in CNRM-CM6-1 and 3–4 days/season in CanESM5) in CDHWD in both the SMILEs. The amplitude and severity of CDHWs exhibit very similar spatial patterns of statistically significant anomalies (CDHWA results are not shown), mostly comparable with the CDHWF results. However, the CDHWS show statistically significantly stronger positive anomalies over the north, northeast, and eastern parts of Australia – similar to CDHWF – and also widespread across southeast and southern regions during the concurrence of strong El Niño with positive IOD phases in CNRM-CM6-1 (Fig. 5). Similarly, CanESM5 results show that positive CDHWS anomalies are stronger over much of the country, particularly during the concurrent strong El Niño and strong positive IOD phase compared to neutral conditions (Supplementary Fig. S3).

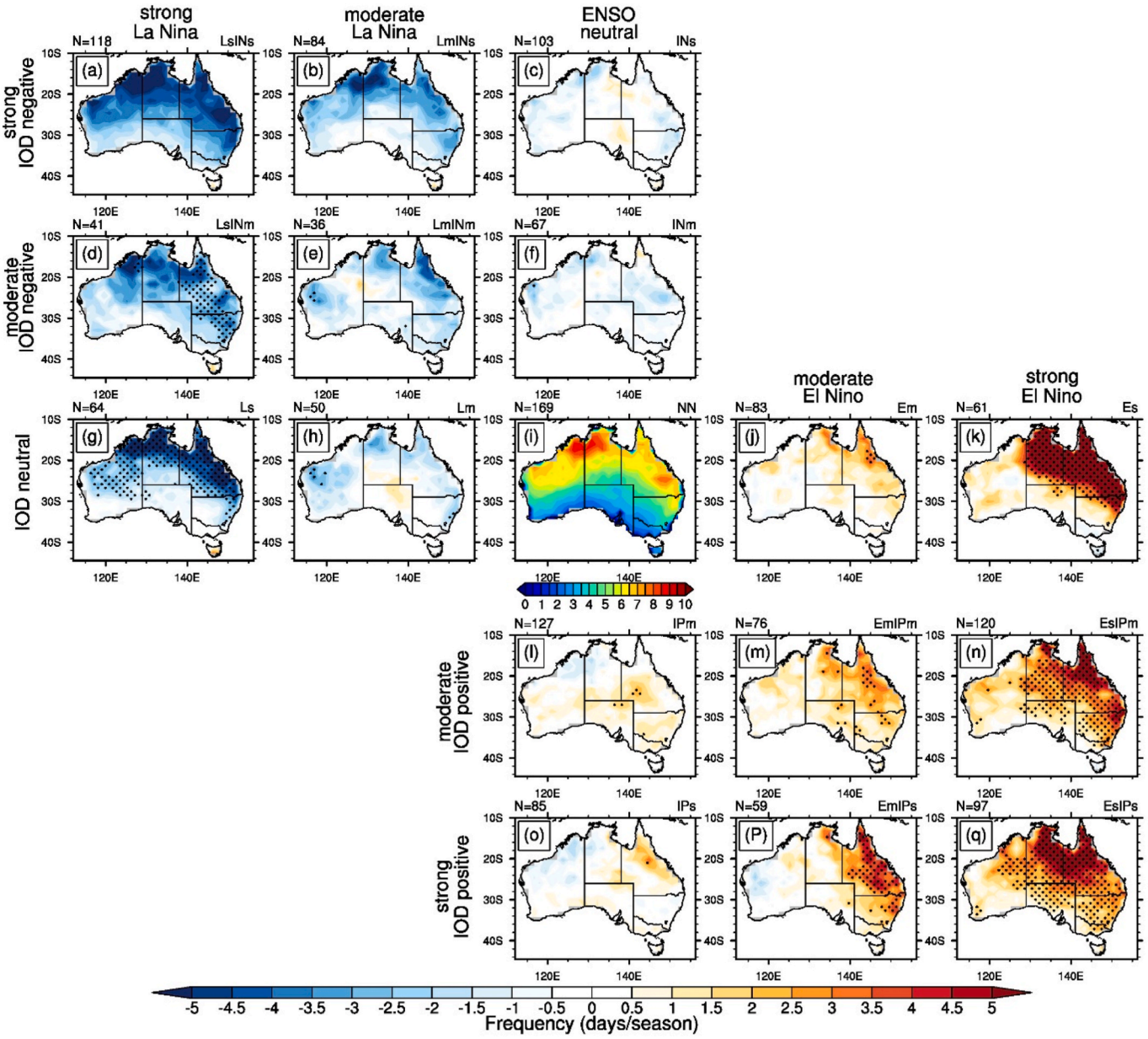

Fig. 4. Composite differences of CDHWF during the various co-occurring phases of ENSO (negative phase on the left increasing to the positive phase on the right) and IOD (negative phase at the top, increasing to the positive phase at the bottom) respective to the neutral conditions (ENSO neutral and IOD neutral, central panel) calculated using CNRM-CM6-1 SMILE. The climatology of CDHWF during the neutral conditions is shown in the centre (i). Drought is defined using SPI-3 ≤ -0.5. The stippled regions represent the difference at the 0.05 significance level. The total number (N) of occurrences of each type of climate mode combination that occurred in the ensemble is shown on the top left of each subplot.

3.3.2. *Variability*

After assessing the influence of different ENSO and IOD phases in the mean of CDHW metrics, this section assesses the spread in CDHW metrics during the same conditions. For this, we focus on the variability of the CDHW metrics (CDHWF and CDHWS) under the ENSO and IOD phases (Figs. 6 and 7 and Supplementary Figs. S4–S5). We calculate variability as the difference between 90th and 10th percentile values of CDHWF during the corresponding co-occurring phases of ENSO and IOD (CNRM-CM6-1 data in Fig. 6 and CanESM5 data in Supplementary Fig. S4). We choose this range (10–90th percentile) as it excludes the outliers and provides a meaningful estimate of spread for both normal and non-normal distributions. Similar to CDHWF, the variabilities of CDHWS during the co-occurring phases of ENSO and IOD using CNRM-CM6-1 data are presented in Fig. 7, and CanESM5 data are shown in Supplementary Fig. S5, respectively.

CDHWF values show substantial variability during the strong El Niño phase and in its concurrence with positive IOD phases, with variability being highest (of about 30 days/season in CNRM-CM6-1 and 40 days/season in CanESM5) in the north of Australia and decreasing when moving further to the south in both SMILEs (see Fig. 6 (k, n, and q) and Supplementary Fig. S4 (k, n, and q)). During these phases, the regions with the large variability in CDHWF also experience strong increases on average (Fig. 4 (k, n, and q) and Supplementary Fig. S2 (k, n, and q)). This means that during strong El Niño and associated positive IOD phases, the mean values of CDHWF are higher than the neutral conditions even when the CDHWF is highly variable, specifically over the north, northeast, and eastern parts of Australia. This suggests that during strong El Niño and concurrence of strong El Niño with positive IOD phases, seasons with a few CDHW days can also occur.

Variability during La Niña phases is lower (by about 10 days/season

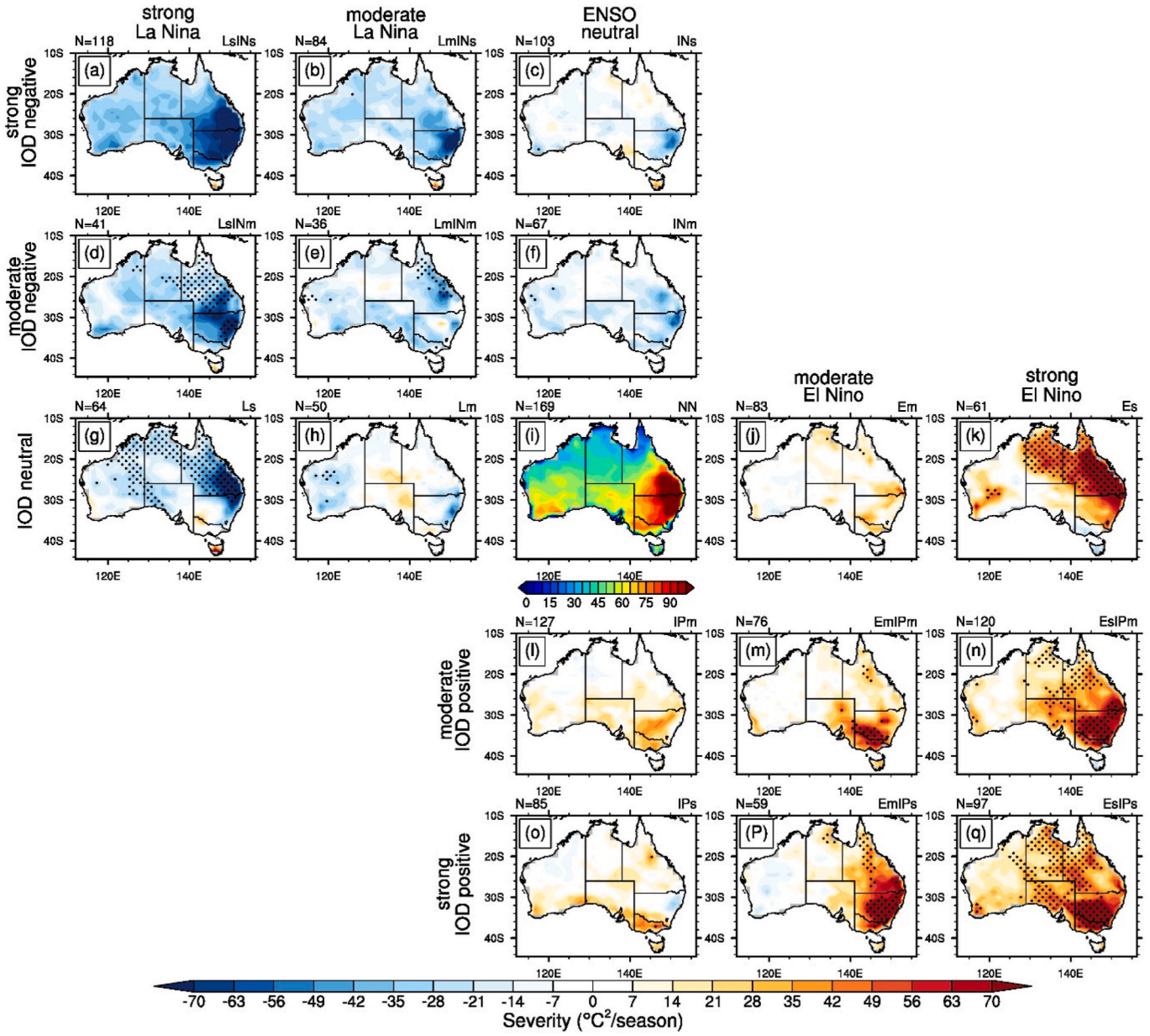

Fig. 5. Same as Fig. 4 but for CDHWS.

in CNRM-CM6-1 and 20 days/season in CanESM5) compared to the neutral conditions, decreasing with the strength of the La Niña event across much of Australia in both SMILEs (see Fig. 6 (g and h) and Supplementary Fig. S4 (g and h)). During the strong La Niña phase, many parts of Australia show lower mean and variability in CDHWF than neutral phase. This suggests that during strong La Niña phases, seasons with fewer CDHW days are highly likely compared to the neutral conditions. Similar results are found for the CDHWD (not shown). The spatial patterns of variability results are found to be similar among CDHWA (not shown) and CDHWS (Fig. 7). Variability of CDHWS on the other hand is highest in the south of Australia (particularly southeast) and decreases when moving northwards during strong El Niño events occurring in isolation or jointly with positive IOD phases in both SMILEs (Fig. 7 (k), (n), and (q) and Supplementary Fig. S5 (k), (n), and (q)).

3.3.3. *Influence on the occurrence of extreme CDHW seasons*

Fig. 8 shows the return period of a season with a CDHWF greater than the 90th percentile of the CDHWF during the neutral phase (hereafter "extreme CDHWF season") for various ENSO and IOD phases using CNRM-CM6-1 SMILE (with CanESM5 shown in Supplementary Fig. S6). We calculate the return period as an inverse of the probability of occurrence of an extreme CDHWF season. Similarly, the return period of extreme CDHWS seasons during the various phases of ENSO and IOD using CNRM-CM6-1 data are presented in Fig. 9, and CanESM5 data are shown in the Supplementary Fig. S7, respectively. Extreme CDHWF seasons are most likely with return periods below two seasons during strong El Niño phases, with the co-occurrence of positive IOD phases (Fig. 8 and Supplementary Fig. S6). This means that during these phases on average for every two seasons there is a chance for the occurrence of extreme CDHWF season. CNRM-CM6-1 results show that during the strong El Niño and concurrence of strong El Niño with positive IOD phases, extreme CDHWF seasons are particularly likely with return periods below two seasons over northeast Australia (Fig. 8 (k, n, and q)). However, CanESM5 suggests that extreme CDHWF seasons are highly likely with return periods below one season over much of Australia, particularly during the co-occurring strong El Niño and strong positive IOD phase (Supplementary Fig. S6 (q)).

Extreme CDHWF seasons are less likely during strong La Niña

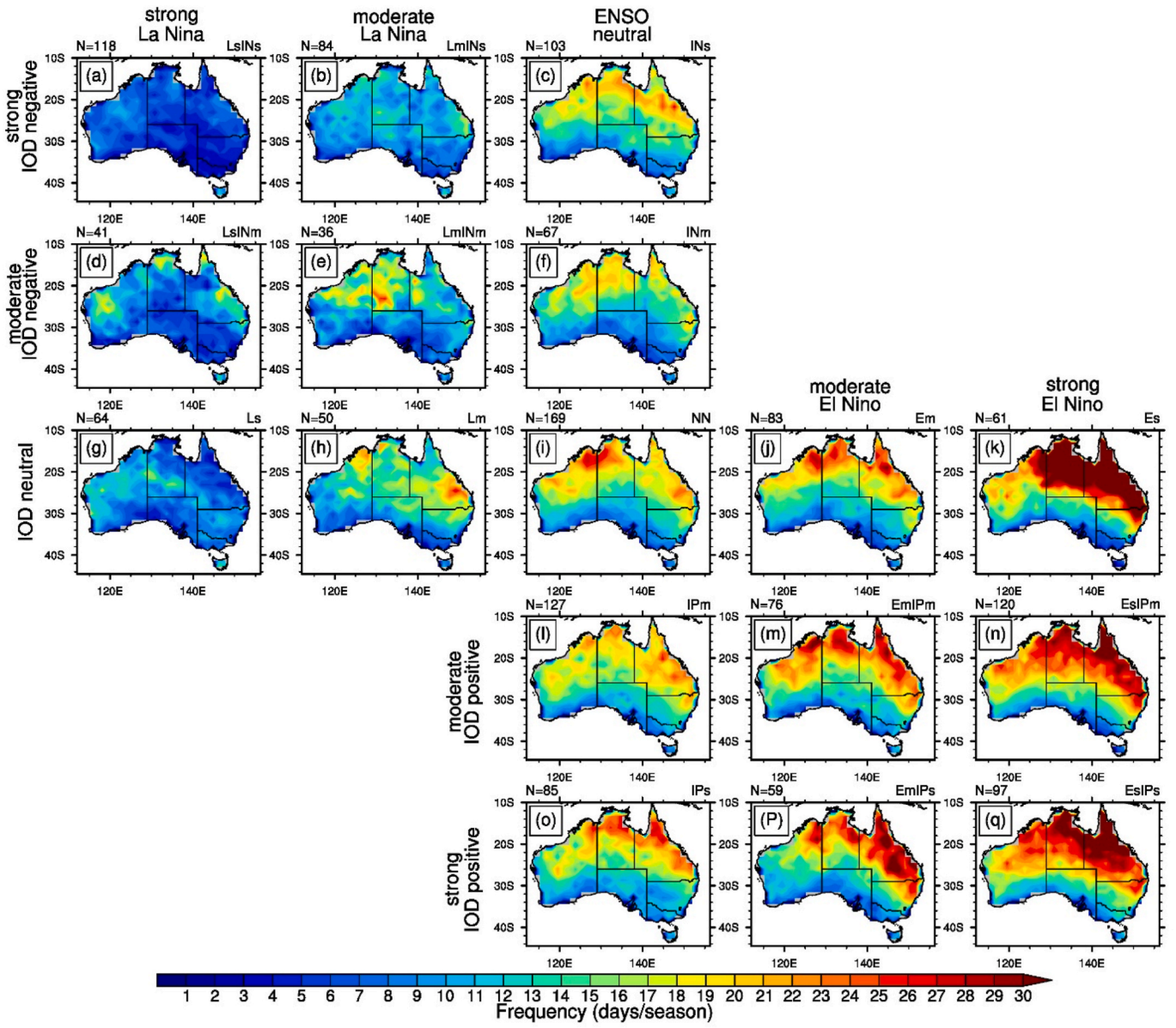

Fig. 6. The difference between the 90th and 10th percentile of CDHWF during the respective co-occurring phases of ENSO and IOD using the CNRM-CM6-1 SMILE data.

seasons, particularly with the co-occurrence of negative IOD phases. For example, CNRM-CM6-1 results suggest that the strong La Niña phase show no occurrences of extreme CDHWF seasons across northeast Australia and the longest return periods (>25 seasons) over much of Australia are seen during the co-occurring strong La Niña and strong IOD negative phase (Fig. 8 (a and g)). CanESM5 shows longest return periods (>25 seasons) during the strong La Niña phase and no occurrences of extreme CDHWF seasons during the co-occurring strong La Niña and strong IOD negative phase over much of Australia (Supplementary Figs. S6(a and g)). These CDHWF results are very similar to CDHWD (not shown) and partly comparable with CDHWA (not shown) and CDHWS (Fig. 9 and Supplementary Fig. S7). However, other than for extreme CDHWF, extreme CDHWS seasons show return periods below two seasons over south-eastern Australia in CNRM-CM6-1, particularly during the concurrence of El Niño seasons with the positive phases of IOD (Fig. 9 (n and q)). While CanESM5 shows a return period of one season over much of Australia during the co-occurring strong El Niño and strong IOD positive phase (Supplementary Fig. S7 (q)).

3.3.4. *Land surface conditions*

Our results suggest that CDHW characteristics are strongly influenced during the strong El Niño, the concurrence of strong El Niño with both the moderate and strong positive IOD, and strong La Niña phases compared to the neutral conditions (Figs. 4–9). Many previous studies suggest that land surface conditions play a critical role in affecting the droughts and heatwaves in Australia (Herold et al., 2016; Hirsch et al., 2019; Holgate et al., 2020; Perkins et al., 2015). The response of land surface conditions to strong El Niño, the concurrence of strong El Niño with both the moderate and strong positive IOD, and strong La Niña phases might have influenced the CDHW activity. To examine this, we have analysed the composite differences of evaporative fraction (EF) between these phases and the neutral phase (CNRM-CM6-1 data in Fig. 10 and CanESM5 data in Supplementary Fig. S9). Detrending the EF had a minimal effect on the results. For the purposes of this study, we only show the results obtained without removing the trend from EF data. The evaluation of the CNRM-CM6-1 and CanESM5 model's skill in simulating EF over Australia is presented in Supplementary Fig. S8. In comparison with EF climatology of 20CR data, CNRM-CM6-1 is able to

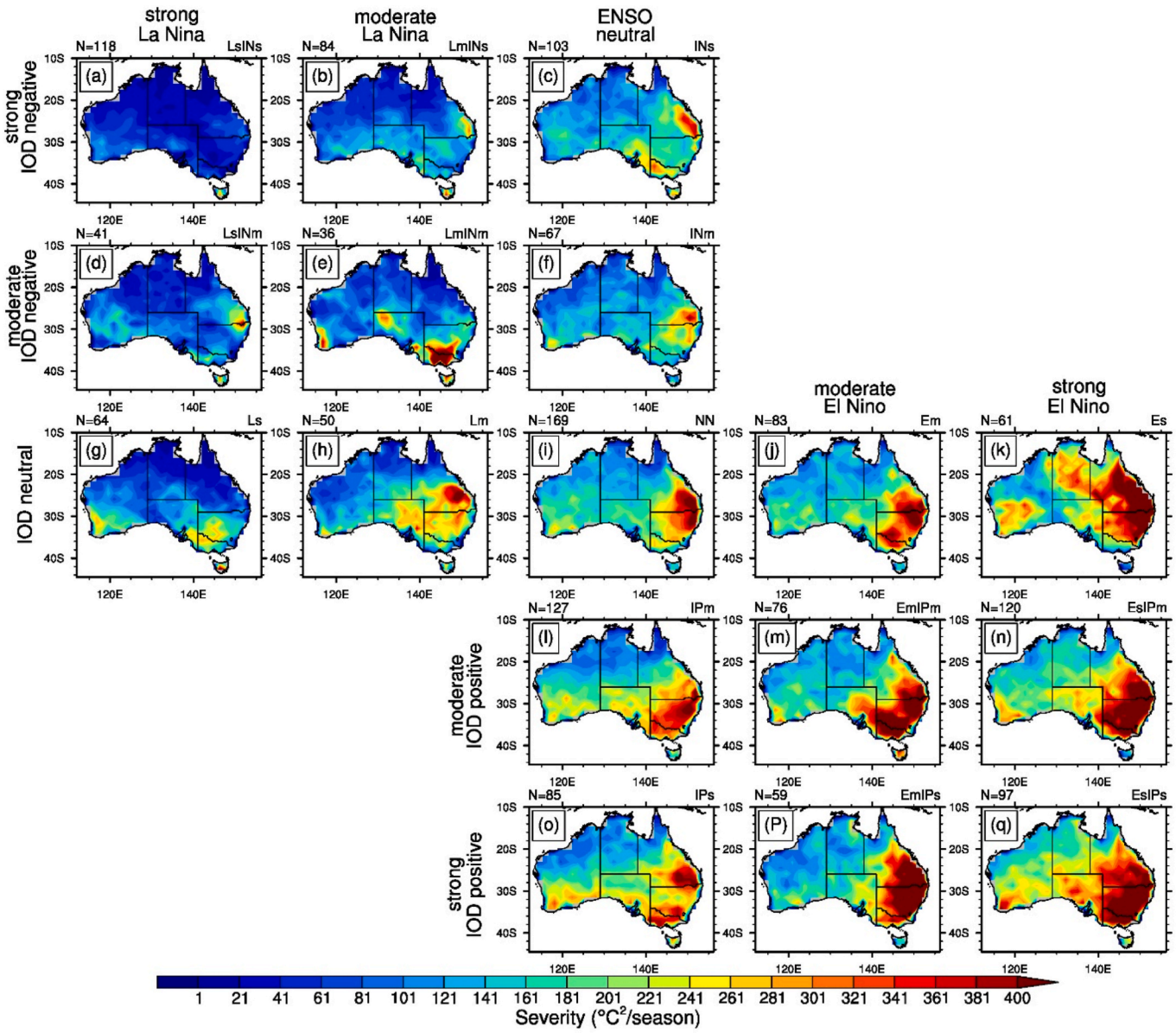

Fig. 7. Same as Fig. 6 but for CDHWS.

capture the spatial variations of the EF over Australia reasonably well (see Supplementary Fig. S8 (a and b)). However, CNRM-CM6-1 shows positive biases in EF, particularly across central Australian regions (Supplementary Fig. S8 (a and b)). The positive biases in EF can induce the risk of underestimating the positive land-atmosphere feedback mechanisms, thus leading to underestimating average CDHW conditions. The CanESM5 model shows negative biases in EF over Australia's northern and eastern coastal regions, which suggests the overestimation of positive land-atmosphere coupling and the exacerbation of CDHW conditions in those regions (Supplementary Fig. S8 (c)).

The statistically significant lower EF values are seen during the strong El Niño phase compared to the neutral, particularly over Australia's eastern and northeastern coasts in the CNRM-CM6-1 (Fig. 10 (a)) and over much of Australia except the northern region in the CanESM5 (Supplementary Fig. 9 (a)). These low EF values are seen over the northeastern and southeastern Australia during concurrent strong El Niño and moderate IOD positive and are widespread over the northern, northeast, and southeast Australia during the co-occurring strong El Niño and strong IOD positive phase in the CNRM-CM6-1 (Fig. 10 (b and c)). However, CanESM5 shows statistically significant low EF values over much of Australia during the co-occurring strong El Niño and strong IOD positive phase, particularly with greater negative anomalies over northeastern and southeastern Australia (Supplementary Fig. 9 (c)). The regions that show statistically significant low EF values during the strong El Niño, the concurrence of strong El Niño with positive IOD phases (Fig. 10 (a–c)) also exhibit statistically significant high CDHW characteristics (particularly severity) in those phases, respectively (Figs. 4 and 5 (k, n, and q)). The low EF values indicate the dry land surface conditions and an increase in the rate of atmosphere warming by the land surface (Gibson et al., 2017; Loughran et al., 2019). In contrast, the statistically significant higher EF values are seen whole over Australia except the western region during the strong La Niña phase compared to the neutral phase in both the SMILEs (Fig. 10 (d) and Supplementary Fig. S9 (d)). The greater EF values are seen particularly across northeast and northern regions during the strong La Niña phase, and in these regions, statistically significant low CDHW characteristics (mainly frequency) (Fig. 4 (g)) and no occurrences of extreme CDHW season are also observed (Figs. 8 and 9 (g)).

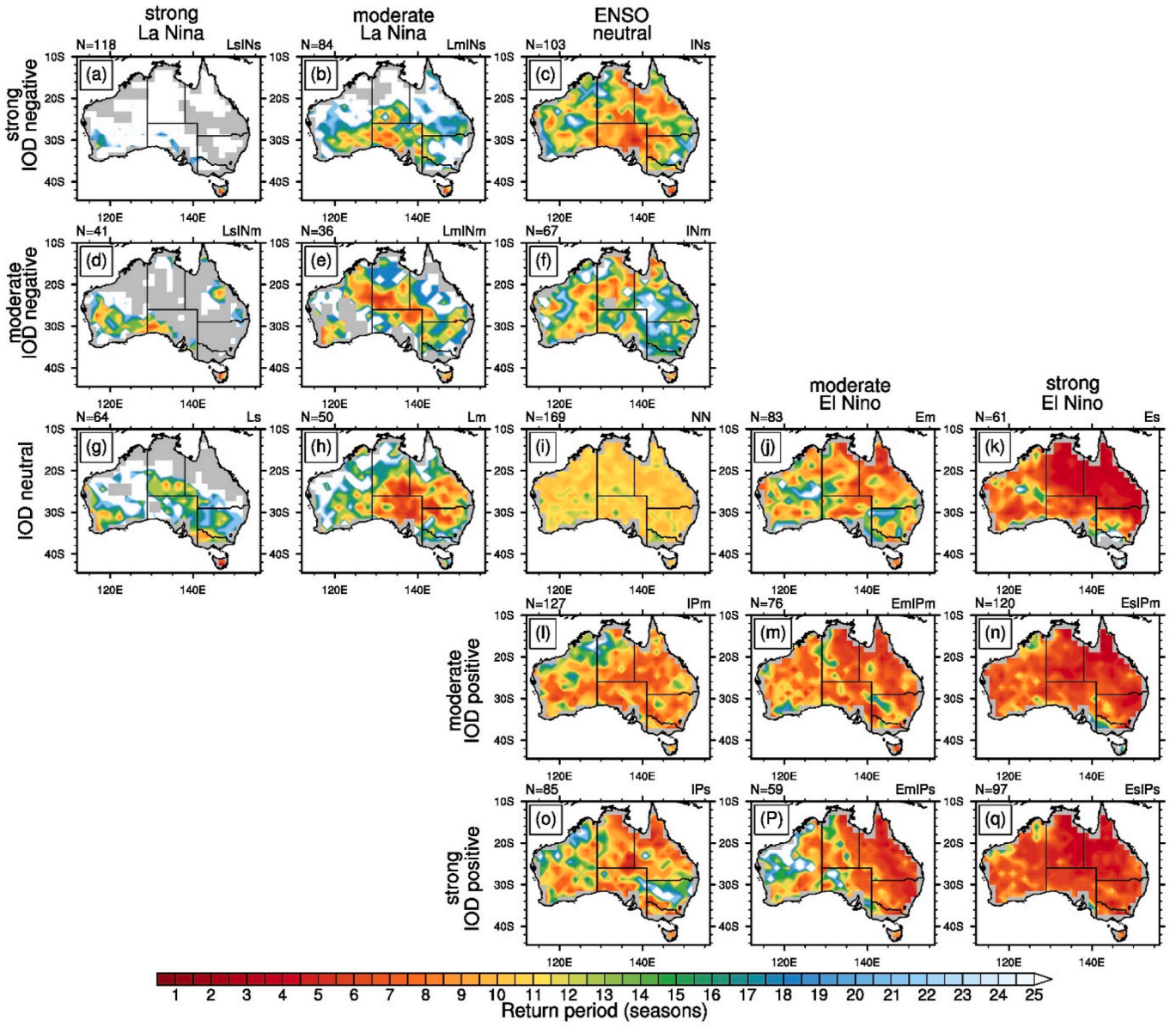

Fig. 8. Return period of extreme CDHWF season during the various phases of ENSO and IOD using the CNRM-CM6-1 SMILE data. Here the extreme CDHWF season refers to a season where CDHWF is greater than the 90th percentile value of CDHWF during the neutral (NN) phase. Grey areas represent no occurrences of extreme CDHWF seasons.

4. Discussion and conclusions

This study, for the first time, quantified observed changes in CDHW characteristics over Australia in the extended summer under past warming conditions. Our results show that CDHW events are occurring more frequently and become longer and more severe under warmer conditions, particularly over eastern Australia (Fig. 2). These observational results can contain biases which could have occurred during the gridding process of station data in producing a gridded dataset (Jones et al., 2009; Reddy et al., 2021b). However, AGCD/AWAP gridded data is known to be a reliable dataset for Australia due to its high station density and has been widely used in previous studies of temperature and precipitation extremes (Gallant et al., 2013; Reddy et al., 2021b; Perkins et al., 2015). Our qualitative results are therefore most likely to hold using alternative observational datasets (like HadGHCND (Caesar et al., 2006) and Berkeley Earth (Rohde et al., 2013) global observational datasets).

To assess the impact of large-scale climate modes of variability on CDHW characteristics, we focused on ENSO and IOD and their combinations for the historical period 1958–2014 in Australia using data from the CMIP6 SMILEs project (CNRM-CM6-1 and CanESM5). Using climate model data, our analysis suggests that results contain model-specific biases. For instance, CNRM-CM6-1 shows positive biases in the magnitude of CDHW metrics across eastern parts of Australia and underestimates their variability over southern parts (Fig. 3), while CanESM5 overestimates the CDHW metrics and their variability over many parts of Australia (Supplementary Fig. S1). These results are consistent with previous studies, which showed that CanESM5 simulated extreme temperatures that were hotter than CNRM-CM6-1 across Australia (Deng et al., 2021). In terms of climate modes, CNRM-CM6-1 has satisfactorily reproduced tropical SSTs and their global teleconnections (Voldoire et al., 2019). Previous studies showed that CNRM-CM6-1 SMILE members simulated the extreme temperatures and drought characteristics (duration and intensity) well within the range of CMIP6 models over Australia (Deng et al., 2021; Ukkola et al., 2020). The CanESM5 model has well represented the tropical SSTs but with

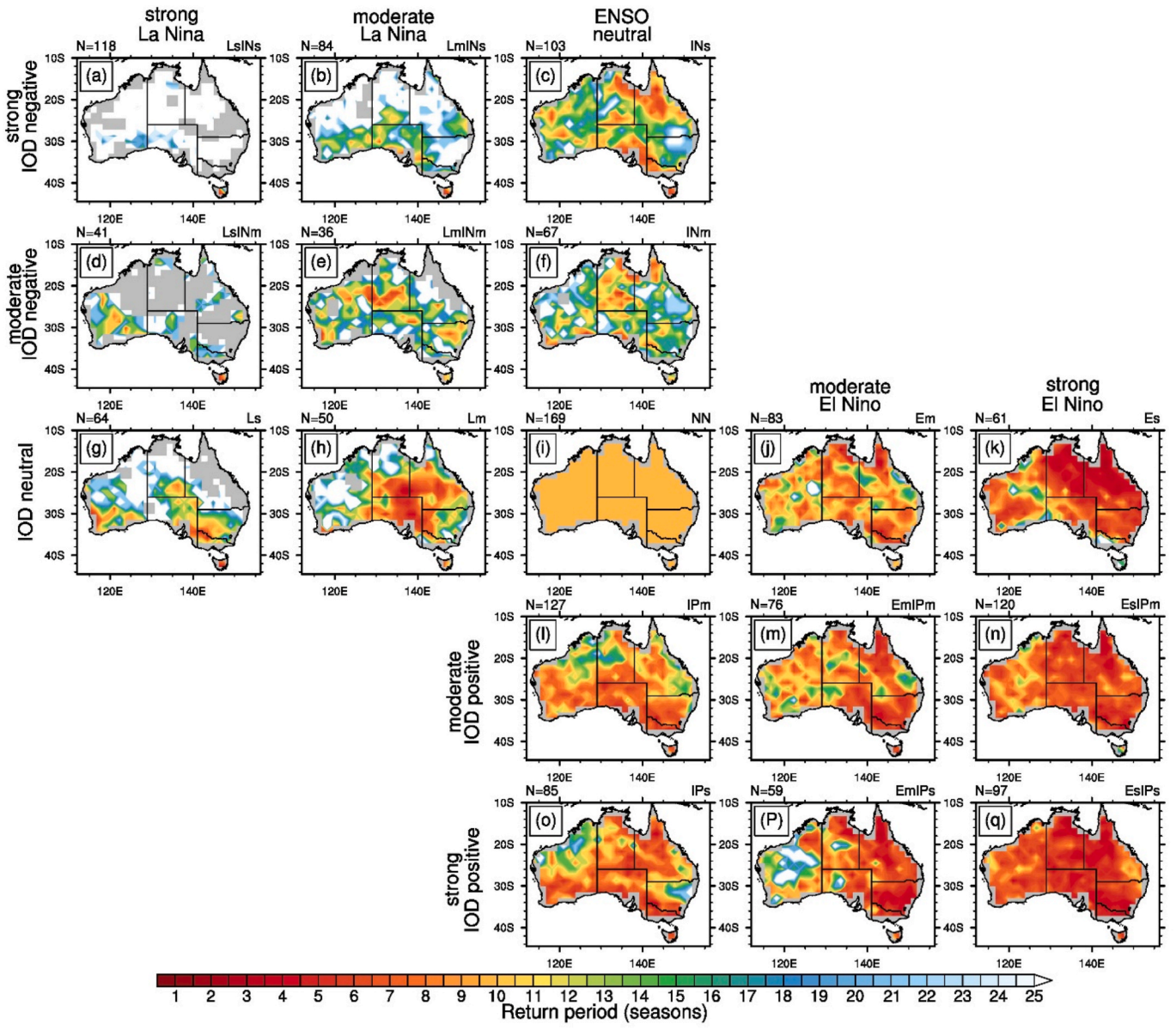

Fig. 9. Same as Fig. 8 but for CDHWS.

slightly weaker ENSO teleconnections compared to HadISST observations (Swart et al., 2019). The CanESM5 model shows reasonable skill in simulating the heatwave-drought compounds over Australia compared to the CMIP6 multi-model mean, with positive biases over northern Australia (Ridder et al., 2021). Overall, it is reasonable to assume that our results could be reproduced by other climate models; however, this requires further examination.

This study is the first to systematically quantify the association between co-occurring phases of ENSO and IOD and CDHW characteristics of the extended summer season over Australia using the two CMIP6 SMILEs. Our results show that CDHWs are dominated mainly by ENSO, with El Niño causing more frequent, prolonged, and severe events, particularly over north and eastern Australia. La Niña has the opposite effect, while the IOD has a smaller impact on CDHW characteristics. The minimal impact of IOD could be because the focus is on the extended summer season CDHW metrics and the IOD typically degenerates by November. These results are in line with previous studies, which show that El Niño has a significant favourable influence on the occurrence of austral summer CDHWs over Australia and southern Africa (Hao et al., 2018; Mukherjee et al., 2020). Furthermore, our results show more frequent and intense CDHWs are widespread across much of Australia except western Australia during the concurrence of strong El Niño with positive phases of IOD than in strong El Niño phase (Figs. 4 and 5 (n and q) and Supplementary Figs. S2–S3 (n and q)). This highlights the importance of considering ENSO and IOD combinations rather than understanding their influence independently on CDHWs in Australia. Our results are consistent with previous studies, which showed that concurrence of El Niño with the positive phase of IOD seasons are associated with cool-season (June–October) drought conditions over southeast Australia (Ummenhofer et al., 2011) and extended summer large contiguous heatwaves (Reddy et al., 2021c) in Australia. Moreover, our results show that the regional influence of co-occurring strong El Niño with moderate IOD positive and strong IOD positive phases is not consistent across the frequency and severity of CDHWs. Even though statistically significant increases in both CDHW frequency and severity are seen across much of Australia during the co-occurrence of strong El Niño with positive IOD phases, the strongest signal in the frequency of CHDWs is seen particularly over the northern tropical and subtropical regions (Fig. 4 (n and q)). In contrast, the strongest signal in CDHW severity is seen mainly across southeast Australia during the

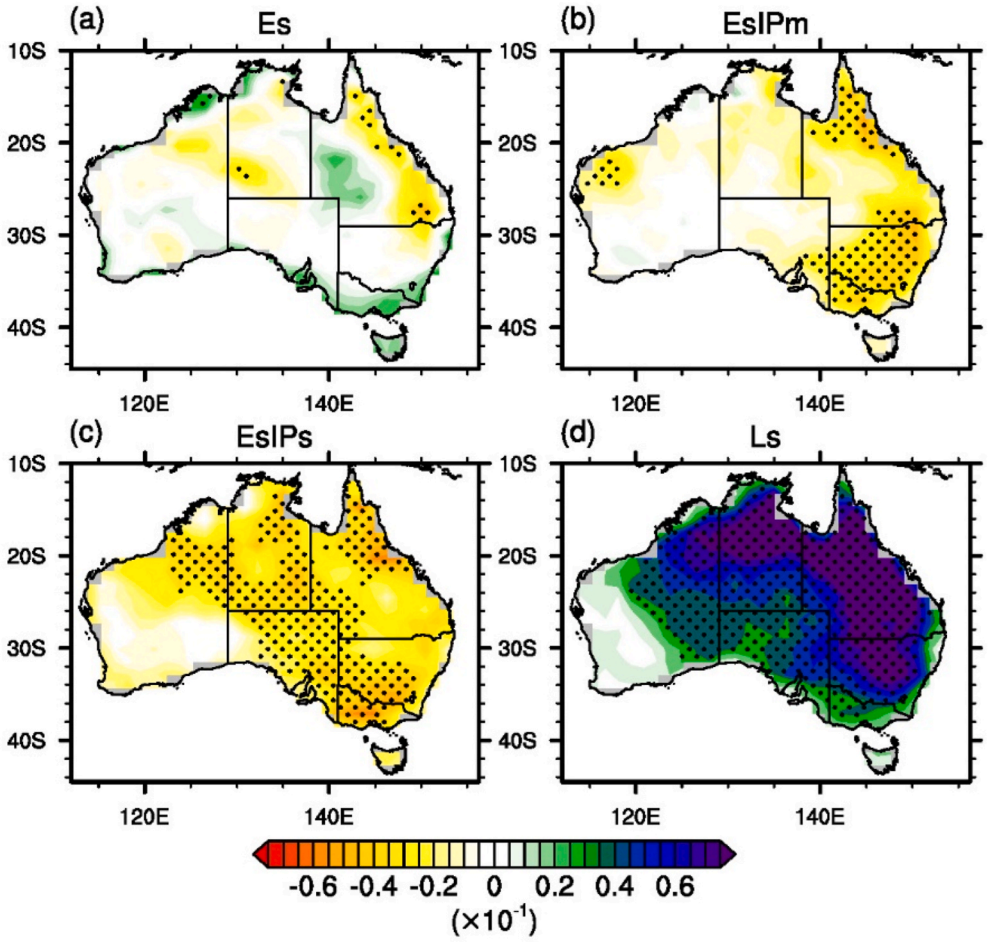

Fig. 10. Composite differences of evaporative fraction (EF) between (a) strong El Niño, (b) co-occurring strong El Niño and moderate IOD positive, (c) co-occurring strong El Niño and strong IOD positive, and (d) strong La Niña phases and the neutral phase, respectively calculated using CNRM-CM6-1 SMILE. The stippled regions represent the difference at the 0.05 significance level.

concurrence of strong El Niño with positive IOD phases (Fig. 5 (n and q)). This highlights the significance of considering various CDHW characteristics in investigating their association with ENSO and IOD combinations over Australia. Although strong El Niño and positive IOD combinations are associated with widespread increases in CDHW characteristics, the co-occurrence of negative IOD phases with strong La Niña fails to similarly produce more widespread statistically significant signals (Figs. 4 and 5). This implies asymmetrical responses of CDHWs to ENSO and IOD combinations. The ENSO-IOD asymmetrical impact on CDHWs might be due to the stronger link of El Niño and IOD positive combination than the La Niña and negative IOD (Cai et al., 2012), which needs further investigation.

ENSO and IOD trigger the background atmospheric processes that are favourable for the occurrence of frequent, persistent, and intense heatwaves across Australia (Loughran et al., 2019; Perkins et al., 2015). Land-atmosphere feedbacks and synoptic systems are the key background physical mechanisms that drive the coupling between droughts and heatwaves (Miralles et al., 2019). The dry land surface conditions with dominating surface sensible heat flux warm the near-surface atmosphere and favour the positive land-atmosphere feedback mechanism (Alexander, 2011). The responsive land-atmosphere coupling further dries the land surface and enhances heat accumulation in the near-surface atmosphere. Previous studies have identified that over-responsive land-atmosphere coupling amplifies the heatwaves and droughts in Australia (Herold et al., 2016; Hirsch et al., 2019; Holgate et al., 2020). However, the response of heatwaves to dry land surface conditions varies regionally, such that northern Australian heatwaves are more responsive to the local dry land surface, whereas heatwaves in southern Australia are less responsive (Hirsch et al., 2019). The role of local land surface conditions in influencing the droughts and heatwaves is not limited to local regions but can impact the remote regions. For example, Holgate et al. (2020) show that the land desiccation in the northern regions of the Murray Darling basin amplifies the droughts in the southern regions of the basin by the reduction in moisture transport; this could result in the intensification of heatwave as well. The local dry land surface conditions can trigger the formation of CDHWs locally and in remote locations through the local and teleconnected land-atmosphere feedbacks (Miralles et al., 2019).

Our results show that co-occurring strong El Niño and strong positive IOD phase is linked with statistically significant dry land surface conditions across much of Australia except western Australia compared to neutral conditions (Fig. 10 (b and c) and supplementary fig. S8 (b-c)). Previous studies show that co-occurring strong El Niño with the strong positive phase of IOD is associated with statistically significant high-pressure anomalies over much of Australia compared to the neutral conditions (Reddy et al., 2022). Gibson et al. (2017) identified that dry land surface conditions in concurrence with the high-pressure circulation features enhance the probability of heatwave occurrence over Australia. Therefore, the dry land surface conditions and high-pressure anomalies associated with co-occurring strong El Niño and strong positive IOD phase could have favoured the more widespread increases in frequency and severity of CDHWs over much of Australia through the local and teleconnected land-atmosphere feedbacks. However, a further investigation on the role of land surface conditions and high-pressure

circulations in influencing the CDHWs over Australia is required. Future studies can focus on the specific CDHW events for a deeper understanding of their background physical mechanisms, which is out of the scope of the present study. During both the moderate and strong El Niño and its associated positive IOD phases, the CDHW metrics are highly variable, specifically the CHDWF over the northeast and the CDHWS over the southeast of Australia (Figs. 6 and 7 (j, k, m, n, p, q)). This variability might be occurred due to the diversifying influence of El Niño event types (central Pacific El Niño and eastern Pacific El Niño) on Australian rainfall (Freund et al., 2021), which needs further investigation. This can be analysed by further separating El Niño into central Pacific El Niño and eastern Pacific El Niño, which is outside the scope of the present study.

In contrast to strong El Niño, our results show strong La Niña phase is associated with the wet land surface conditions across most of Australia except the western region, and in particular, more wetter conditions are seen over northeast Australia (Fig. 10 (d) and Supplementary Fig. S9 (d)). These wet land surface conditions with dominating surface latent heat flux promote cloud formation in the lower atmosphere and cool the surface (Alexander, 2011). Previous studies suggested that land-atmosphere feedbacks are overestimated by most of the climate models (Ukkola et al., 2018), which may have influenced the frequency and severity of CDHWs. However, previous observational studies showed that extreme heatwave seasons are less likely to occur in Australia during the wet land surface conditions (Herold et al., 2016; Perkins et al., 2015). Our results broadly agree with these previous studies and show no occurrences of extreme CDHW seasons during the strong La Niña phase over northeast Australia (Figs. 8 and 9 (g)), where the wet land surface conditions are seen (Fig. 10 (d)).

We focus on ENSO and IOD due to their predominant influence on Australian precipitation and temperature extremes. Other modes of climate variability, such as the Madden-Julian Oscillation (MJO), the Southern Annular Mode (SAM), and the Interdecadal Pacific Oscillation (IPO), also influence Australian temperature and precipitation extremes and interact with ENSO and IOD (Dey et al., 2021; Loughran et al., 2017a; Marshall et al., 2014, 2021). Future research could consider the combinations of these other climate drivers and their combined impacts on CDHWs in Australia. Recent studies show that two different El Niño types, namely central Pacific El Niño and eastern Pacific El Niño, have varying influences on the Australian rainfall (Freund et al., 2021; Wiedermann et al., 2021). In contrast, Loughran et al. (2017b) found that there is no significant difference between the influence of two El Niño types on Australian heatwaves. However, further research is required in investigating the impacts of two El Niño types on CDHWs in Australia, which may also consider the combinations of two El Niño types with other modes of variability (such as IOD, MJO, SAM, and IPO). Nevertheless, our results can provide useful information in understanding the large-scale climate drivers of Australian CDHWs and thus can help in improving their seasonal scale predictability.

In this study, we have only considered meteorological droughts in defining the CDHWs. Recent studies showed that the ongoing meteorological drought can rapidly intensify within a few weeks and can lead to the formation of flash droughts or vice versa (Nguyen et al., 2019, 2021; Parker et al., 2021). Heatwaves can initiate flash droughts, and then flash droughts can further amplify and prolong the heatwave conditions (Christian et al., 2020; Parker et al., 2021). Identifying the clear association between flash drought and heatwaves and linking their compound occurrences with climate variability modes is important to study because of their severe agricultural impacts (Parker et al., 2021), but it is out of the scope of the present study. In the future, one can consider separating the flash droughts from meteorological droughts and can implement the present study's approach in understanding their driving mechanisms.

In conclusion, our results present information on climate variability modes favouring CDHWs, which signify conditions that have the potential to cause severe socio-economic and ecological impacts. Furthermore, our results show that east Australia is particularly vulnerable to a worsening of CDHW conditions in a warming climate. The eastern Australian seaboard is particularly important for the country's economy and has the highest population numbers. As such, increases in CDHW events over eastern Australia have significant implications for the national economy (Horridge et al., 2005), crop yield (Herold et al., 2018), labour productivity, and bushfire potential (Abram et al., 2021; Reddy et al., 2021a). Therefore, our results are an important step in preparing Australia for future hazardous conditions projected to be aggravated under future warming.

Credit author statement

P. Jyoteeshkumar reddy: Conceptualization, Methodology, Formal analysis, Software, Visualization, Writing- Original draft preparation. **Sarah E. Perkins-Kirkpatrick:** Supervision, Conceptualization, Methodology, Writing- Reviewing and Editing. **Nina N. Ridder**: Supervision, Methodology, Writing- Reviewing and Editing. **Jason J. Sharples**: Supervision, Writing- Reviewing and Editing.

Declaration of competing interest

The authors declare that they have no known competing financial interests or personal relationships that could have appeared to influence the work reported in this paper.

Acknowledgments

The authors would like to thank two anonymous reviewers for their constructive comments, which helped improve the manuscript's quality. The authors thank the Bureau of Meteorology and CSIRO for making the AGCD/AWAP observational gridded dataset available. We thank the U. K. Hadley Centre for providing the HadISST v1.1 data. The authors thank CNRM/CERFACS and the Canadian Centre for Climate Modelling and Analysis modelling groups for producing and making available CNRM-CM6-1 and CanESM5 models data. We thank the U.S. Department of Energy, Office of Science Biological and Environmental Research, and the National Oceanic and Atmospheric Administration Climate Program Office for providing the NOAA-CIRES 20CR version 2c dataset. S. E. Perkins-Kirkpatrick is supported by ARC grant (FT170100106). S. E. Perkins-Kirkpatrick and N. N. Ridder are supported by the ARC CLEX grant (CE170100023).

Appendix A. Supplementary data

Supplementary data to this article can be found online at https://doi.org/10.1016/j.wace.2022.100469.

References

Abram, N.J., Henley, B.J., Gupta sen, A., Lippmann, T.J.R., Clarke, H., Dowdy, A.J., Sharples, J.J., Nolan, R.H., Zhang, T., Wooster, M.J., Wurtzel, J.B., Meissner, K.J., Pitman, A.J., Ukkola, A.M., Murphy, B.P., Tapper, N.J., Boer, M.M., 2021. Connections of climate change and variability to large and extreme forest fires in southeast Australia. Commun. Earth Environ. (1 2), 1–17. https://doi.org/10.1038/s43247-020-00065-8, 2021 2.

Administration References Committee, P., 2019. Lessons to Be Learned in Relation to the Australian Bushfire Season 2019-20.

Alexander, L., 2011. Extreme heat rooted in dry soils. Nat. Geosci. 4, 12–13. https://doi.org/10.1038/ngeo1045.

Allen, C.D., Macalady, A.K., Chenchouni, H., Bachelet, D., McDowell, N., Vennetier, M., Kitzberger, T., Rigling, A., Breshears, D.D., Hogg, E.H., Ted), Gonzalez, P., Fensham, R., Zhang, Z., Castro, J., Demidova, N., Lim, J.H., Allard, G., Running, S. W., Semerci, A., Cobb, N., 2010. A global overview of drought and heat-induced tree mortality reveals emerging climate change risks for forests. For. Ecol. Manag. 259, 660–684. https://doi.org/10.1016/J.FORECO.2009.09.001.

Baldwin, J.W., Dessy, J.B., Vecchi, G.A., Oppenheimer, M., 2019. Temporally compound heat wave events and global warming: an emerging hazard. Earth's Future 7, 411–427. https://doi.org/10.1029/2018EF000989.

Caesar, J., Alexander, L., Vose, R., 2006. Large-scale changes in observed daily maximum and minimum temperatures: creation and analysis of a new gridded data set. J. Geophys. Res. Atmos. 111 https://doi.org/10.1029/2005JD006280.

Cai, W., van Rensch, P., Cowan, T., Hendon, H.H., 2012. An asymmetry in the IOD and ENSO teleconnection pathway and its impact on Australian climate. J. Clim. 25, 6318–6329. https://doi.org/10.1175/JCLI-D-11-00501.1.

Casselman, J.W., Taschetto, A.S., Domeisen, D.I. v, 2021. Non-linearity in the pathway of El niño-southern oscillation to the tropical north atlantic. J. Clim. 34 (17), 7277–7296. https://doi.org/10.1175/JCLI-D-20-0952.1.

Christian, J.I., Basara, J.B., Hunt, E.D., Otkin, J.A., Xiao, X., 2020. Flash drought development and cascading impacts associated with the 2010 Russian heatwave. Environ. Res. Lett. 15, 094078 https://doi.org/10.1088/1748-9326/AB9FAF.

Ciais, Ph, Reichstein, M., Viovy, N., Granier, A., Ogée, J., Allard, V., Aubinet, M., Buchmann, N., Bernhofer, Chr, Carrara, A., Chevallier, F., de Noblet, N., Friend, A. D., Friedlingstein, P., Grünwald, T., Heinesch, B., Keronen, P., Knohl, A., Krinner, G., Loustau, D., Manca, G., Matteucci, G., Miglietta, F., Ourcival, J.M., Papale, D., Pilegaard, K., Rambal, S., Seufert, G., Soussana, J.F., Sanz, M.J., Schulze, E.D., Vesala, T., Valentini, R., 2005. Europe-wide reduction in primary productivity caused by the heat and drought in 2003. Nature 437, 529–533. https://doi.org/10.1038/nature03972, 2005 437:7058.

Coffel, E.D., Keith, B., Lesk, C., Horton, R.M., Bower, E., Lee, J., Mankin, J.S., 2019. Future hot and dry years worsen nile basin water scarcity despite projected precipitation increases. Earth's Future 7, 967–977. https://doi.org/10.1029/2019EF001247.

Compo, G.P., Whitaker, J.S., Sardeshmukh, P.D., Matsui, N., Allan, R.J., Yin, X., Gleason, B.E., Vose, R.S., Rutledge, G., Bessemoulin, P., Brönnimann, S., Brunet, M., Crouthamel, R.I., Grant, A.N., Groisman, P.Y., Jones, P.D., Kruk, M., Kruger, A.C., Marshall, G.J., Maugeri, M., Mok, H.Y., Nordli, Ø., Ross, T.F., Trigo, R.M., Wang, X. L., Woodruff, S.D., Worley, S.J., 2011. The twentieth century reanalysis project. Quarterly J. Roy. Meteorol. Soc. 137, 1–28. https://doi.org/10.1002/qj.776.

DelSole, T., Trenary, L., Tippett, M.K., Pegion, K., 2017. Predictability of week-3-4 average temperature and precipitation over the contiguous United States. J. Clim. 30, 3499–3512. https://doi.org/10.1175/JCLI-D-16-0567.1.

Deng, X., Perkins-Kirkpatrick, S.E., Lewis, S.C., Ritchie, E.A., 2021. Evaluation of extreme temperatures over Australia in the historical simulations of CMIP5 and CMIP6 models. Earth's Future 9, e2020EF001902. https://doi.org/10.1029/2020EF001902.

Dey, R., Bador, M., Alexander, L.v., Lewis, S.C., 2021. The drivers of extreme rainfall event timing in Australia. Int. J. Climatol. 41, 6654–6673. https://doi.org/10.1002/JOC.7218.

Donat, M.G., Pitman, A.J., Seneviratne, S.I., 2017. Regional warming of hot extremes accelerated by surface energy fluxes. Geophys. Res. Lett. 44, 7011–7019. https://doi.org/10.1002/2017GL073733.

Esfahanian, E., Nejadhashemi, A.P., Abouali, M., Adhikari, U., Zhang, Z., Daneshvar, F., Herman, M.R., 2017. Development and evaluation of a comprehensive drought index. J. Environ. Manag. 185, 31–43. https://doi.org/10.1016/J.JENVMAN.2016.10.050.

Fink, A.H., Brücher, T., Krüger, A., Leckebusch, G.C., Pinto, J.G., Ulbrich, U., 2004. The 2003 European summer heatwaves and drought –synoptic diagnosis and impacts. Weather 59, 209–216. https://doi.org/10.1256/WEA.73.04.

Fischer, E.M., Schär, C., 2010. Consistent geographical patterns of changes in high-impact European heatwaves. Nat. Geosci. 3, 398–403. https://doi.org/10.1038/ngeo866.

Ford, T.W., Wulff, C.O., Quiring, S.M., 2014. Assessment of observed and model-derived soil moisture-evaporative fraction relationships over the United States Southern Great Plains. J. Geophys. Res. Atmos. 119, 6279–6291. https://doi.org/10.1002/2014JD021490.

Freund, M.B., Marshall, A.G., Wheeler, M.C., Brown, J.N., 2021. Central pacific El Niño as a precursor to summer drought-breaking rainfall over southeastern Australia. Geophys. Res. Lett. 48, e2020GL091131 https://doi.org/10.1029/2020GL091131.

Gallant, A.J.E., Reeder, M.J., Risbey, J.S., Hennessy, K.J., 2013. The characteristics of seasonal-scale droughts in Australia, 1911–2009. Int. J. Climatol. 33, 1658–1672. https://doi.org/10.1002/JOC.3540.

Geirinhas, J.L., Russo, A., Libonati, R., Sousa, P.M., Miralles, D.G., Trigo, R.M., 2021. Recent increasing frequency of compound summer drought and heatwaves in Southeast Brazil. Environ. Res. Lett. 16, 034036 https://doi.org/10.1088/1748-9326/ABE0EB.

Gibson, P.B., Pitman, A.J., Lorenz, R., Perkins-Kirkpatrick, S.E., 2017. The role of circulation and land surface conditions in current and future Australian heat waves. J. Clim. 30, 9933–9948. https://doi.org/10.1175/JCLI-D-17-0265.1.

Good, P., 2013. Permutation Tests: a Practical Guide to Resampling Methods for Testing Hypotheses. Springer Science & Business Media.

Guenang, G.M., Mkankam Kamga, F., 2014. Computation of the standardized precipitation index (SPI) and its use to assess drought occurrences in Cameroon over recent decades. J. Appl. Meteorol. Climatol. 53, 2310–2324. https://doi.org/10.1175/JAMC-D-14-0032.1.

Hao, Z., Hao, F., Singh, V.P., Zhang, X., 2018. Quantifying the relationship between compound dry and hot events and El Niño–southern Oscillation (ENSO) at the global scale. J. Hydrol. 567, 332–338. https://doi.org/10.1016/J.JHYDROL.2018.10.022.

Hayes, M., Svoboda, M., Wall, N., Widhalm, M., 2011. The lincoln declaration on drought indices: universal meteorological drought index recommended. Bull. Am. Meteorol. Soc. 92, 485–488. https://doi.org/10.1175/2010BAMS3103.1.

Herold, N., Kala, J., Alexander, L.v., 2016. The influence of soil moisture deficits on Australian heatwaves. Environ. Res. Lett. 11 (6), 064003 https://doi.org/10.1088/1748-9326/11/6/064003.

Herold, N., Ekström, M., Kala, J., Goldie, J., Evans, J.P., 2018. Australian climate extremes in the 21st century according to a regional climate model ensemble: implications for health and agriculture. Weather Clim. Extrem. 20, 54–68. https://doi.org/10.1016/j.wace.2018.01.001.

Hirsch, A.L., Evans, J.P., di Virgilio, G., Perkins-Kirkpatrick, S.E., Argüeso, D., Pitman, A. J., Carouge, C.C., Kala, J., Andrys, J., Petrelli, P., Rockel, B., 2019. Amplification of Australian heatwaves via local land-atmosphere coupling. J. Geophys. Res. Atmos. 124, 13625–13647. https://doi.org/10.1029/2019JD030665.

Holgate, C.M., van Dijk, A.I.J.M., Evans, J.P., Pitman, A.J., 2020. Local and remote drivers of southeast Australian drought. Geophys. Res. Lett. 47, e2020GL090238 https://doi.org/10.1029/2020GL090238.

Horridge, M., Madden, J., Wittwer, G., 2005. The impact of the 2002–2003 drought on Australia. J. Pol. Model. 27, 285–308. https://doi.org/10.1016/J.JPOLMOD.2005.01.008.

Ionita, M., Caldarescu, D.E., Nagavciuc, V., 2021. Compound hot and dry events in Europe: variability and large-scale drivers. Frontiers in Climate 3, 58. https://doi.org/10.3389/FCLIM.2021.688991.

Jones, D.A., Wang, W., Fawcett, R., 2009. High-quality spatial climate data-sets for Australia. Australian. Meteorol. Oceanogr. J. 58, 233–248. https://doi.org/10.22499/2.5804.003.

Kong, Q., Guerreiro, S.B., Blenkinsop, S., Li, X.F., Fowler, H.J., 2020. Increases in summertime concurrent drought and heatwave in Eastern China. Weather Clim. Extrem. 28 https://doi.org/10.1016/j.wace.2019.100242.

Lehner, F., Deser, C., Maher, N., Marotzke, J., Fischer, E.M., Brunner, L., Knutti, R., Hawkins, E., 2020. Partitioning climate projection uncertainty with multiple large ensembles and CMIP5/6. Earth Syst. Dyn. 11, 491–508. https://doi.org/10.5194/ESD-11-491-2020.

Loughran, T.F., Perkins-Kirkpatrick, S.E., Alexander, L.v., 2017a. Understanding the spatio-temporal influence of climate variability on Australian heatwaves. Int. J. Climatol. 37, 3963–3975. https://doi.org/10.1002/joc.4971.

Loughran, T.F., Perkins-Kirkpatrick, S.E., Alexander, L.v., Pitman, A.J., 2017b. No significant difference between Australian heat wave impacts of Modoki and eastern Pacific El Niño. Geophys. Res. Lett. 44, 5150–5157. https://doi.org/10.1002/2017GL073231.

Loughran, T.F., Pitman, A.J., Perkins-Kirkpatrick, S.E., 2019. The El Niño–Southern Oscillation's effect on summer heatwave development mechanisms in Australia. Clim. Dynam. 52, 6279–6300. https://doi.org/10.1007/s00382-018-4511-x.

Maher, N., Milinski, S., Suarez-Gutierrez, L., Botzet, M., Dobrynin, M., Kornblueh, L., Kröger, J., Takano, Y., Ghosh, R., Hedemann, C., Li, C., Li, H., Manzini, E., Notz, D., Putrasahan, D., Boysen, L., Claussen, M., Ilyina, T., Olonscheck, D., Raddatz, T., Stevens, B., Marotzke, J., 2019. The max planck Institute grand ensemble: enabling the exploration of climate system variability. J. Adv. Model. Earth Syst. 11, 2050–2069. https://doi.org/10.1029/2019MS001639.

Maher, N., Lehner, F., Marotzke, J., 2020. Quantifying the role of internal variability in the temperature we expect to observe in the coming decades. Environ. Res. Lett. 15, 054014 https://doi.org/10.1088/1748-9326/AB7D02.

Maher, N., Milinski, S., Ludwig, R., 2021. Large ensemble climate model simulations: introduction, overview, and future prospects for utilising multiple types of large ensemble. Earth Syst. Dynam. 12, 401–418. https://doi.org/10.5194/esd-12-401-2021.

Marshall, A.G., Hudson, D., Wheeler, M.C., Alves, O., Hendon, H.H., Pook, M.J., Risbey, J.S., 2014. Intra-seasonal drivers of extreme heat over Australia in observations and POAMA-2. Clim. Dynam. 43, 1915–1937. https://doi.org/10.1007/s00382-013-2016-1.

Marshall, A.G., Hendon, H.H., Hudson, D., Marshall, A.G., Hendon, H.H., Hudson, D., 2021. Influence of the Madden-Julian Oscillation on multiweek prediction of Australian rainfall extremes using the ACCESS-S1 prediction system. J. South. Hemisphere Earth Syst. Sci. 71, 159–180. https://doi.org/10.1071/ES21001.

Mazdiyasni, O., AghaKouchak, A., 2015. Substantial increase in concurrent droughts and heatwaves in the United States. Proc. Natl. Acad. Sci. Unit. States Am. 112, 11484–11489. https://doi.org/10.1073/pnas.1422945112.

Mckee, T.B.T.B., Doesken, N.J.N.J., Kleist, J., McKee Doesken, N.J.N.J., Kleist, J., Mckee, T.B.T.B., Doesken, N.J.N.J., Kleist, J., 1993. The relationship of drought frequency and duration to time scales. In: Eighth Conference on Applied Climatology, Anaheim, 17–22, pp. 179–184. January 1993.

Meyers, G., McIntosh, P., Pigot, L., Pook, M., 2007. The years of El Niño, La Niña, and interactions with the tropical Indian ocean. J. Clim. 20, 2872–2880. https://doi.org/10.1175/JCLI4152.1.

Miralles, D.G., Gentine, P., Seneviratne, S.I., Teuling, A.J., 2019. Land–atmospheric feedbacks during droughts and heatwaves: state of the science and current challenges. Ann. N. Y. Acad. Sci. 1436, 19–35. https://doi.org/10.1111/NYAS.13912.

Mo, M., Roache, M., 2021. A review of intervention methods used to reduce flying-fox mortalities in heat stress events. Aust. Mammal. 43, 137–150. https://doi.org/10.1071/AM20038.

Mukherjee, S., Mishra, A.K., 2021. Increase in compound drought and heatwaves in a warming World. Geophys. Res. Lett. 48, e2020GL090617 https://doi.org/10.1029/2020GL090617.

Mukherjee, S., Ashfaq, M., Mishra, A.K., 2020. Compound drought and heatwaves at a global scale: the role of natural climate variability-associated synoptic patterns and land-surface energy budget anomalies. J. Geophys. Res. Atmos. 125, e2019JD031943 https://doi.org/10.1029/2019JD031943.

Nairn, J., Fawcett, R., 2013. Defining Heatwaves: Heatwave Defined as a Heat-Impact Event Servicing All Communiy and Business Sectors in Australia. CAWCR technical report. 551.5250994.

Nguyen, H., Wheeler, M.C., Otkin, J.A., Cowan, T., Frost, A., Stone, R., 2019. Using the evaporative stress index to monitor flash drought in Australia. Environ. Res. Lett. 14, 064016 https://doi.org/10.1088/1748-9326/AB2103.
Nguyen, H., Wheeler, M.C., Hendon, H.H., Lim, E.P., Otkin, J.A., 2021. The 2019 flash droughts in subtropical eastern Australia and their association with large-scale climate drivers. Weather Clim. Extrem. 32, 100321 https://doi.org/10.1016/J.WACE.2021.100321.
Nolan, R.H., Boer, M.M., Collins, L., Resco de Dios, V., Clarke, H., Jenkins, M., Kenny, B., Bradstock, R.A., 2020. Causes and consequences of eastern Australia's 2019–20 season of mega-fires. Global Change Biol. 26, 1039–1041. https://doi.org/10.1111/gcb.14987.
Palmer, W.C., 1965. Meteorological Drought. US Department of Commerce, Weather Bureau.
Parker, T., Gallant, A., Hobbins, M., Hoffmann, D., 2021. Flash drought in Australia and its relationship to evaporative demand. Environ. Res. Lett. 16, 064033 https://doi.org/10.1088/1748-9326/ABFE2C.
Perkins, S.E., Alexander, L.v., 2013. On the measurement of heat waves. J. Clim. 26, 4500–4517. https://doi.org/10.1175/JCLI-D-12-00383.1.
Perkins, S.E., Argüeso, D., White, C.J., 2015. Relationships between climate variability, soil moisture, and Australian heatwaves. J. Geophys. Res. 120, 8144–8164. https://doi.org/10.1002/2015JD023592.
Perkins-Kirkpatrick, S.E., Lewis, S.C., 2020. Increasing trends in regional heatwaves. Nat. Commun. 11, 3357. https://doi.org/10.1038/s41467-020-16970-7.
Pezza, A.B., van Rensch, P., Cai, W., 2012. Severe heat waves in Southern Australia: synoptic climatology and large scale connections. Clim. Dynam. 38, 209–224. https://doi.org/10.1007/s00382-011-1016-2.
Rastogi, D., Lehner, F., Ashfaq, M., 2020. Revisiting recent U.S. Heat waves in a warmer and more humid climate. Geophys. Res. Lett. 47, e2019GL086736 https://doi.org/10.1029/2019GL086736.
Rayner, N.A., Parker, D.E., Horton, E.B., Folland, C.K., Alexander, L.v., Rowell, D.P., Kent, E.C., Kaplan, A., 2003. Global analyses of sea surface temperature, sea ice, and night marine air temperature since the late nineteenth century. J. Geophys. Res. Atmos. 108 https://doi.org/10.1029/2002jd002670.
Reddy, P.J., Sharples, J.J., Lewis, S.C., Perkins-Kirkpatrick, S.E., 2021a. Modulating influence of drought on the synergy between heatwaves and dead fine fuel moisture content of bushfire fuels in the Southeast Australian region. Weather Clim. Extrem. 31, 100300 https://doi.org/10.1016/j.wace.2020.100300.
Reddy, P.J., Perkins-Kirkpatrick, S.E., Sharples, J.J., 2021b. Intensifying Australian heatwave trends and their sensitivity to observational data. Earth's Future 9, e2020EF001924. https://doi.org/10.1029/2020ef001924.
Reddy, P.J., Perkins-Kirkpatrick, S.E., Sharples, J.J., 2021c. Interactive influence of ENSO and IOD on contiguous heatwaves in Australia. Environ. Res. Lett. 17, 014004 https://doi.org/10.1088/1748-9326/ac3e9a.
Reddy, P.J., Perkins-Kirkpatrick, S.E., Sharples, J.J., 2022. Corrigendum: interactive influence of ENSO and IOD on contiguous heatwaves in Australia (2022 Environ. Res. Lett. 17 014004). Environ. Res. Lett. 17, 049501 https://doi.org/10.1088/1748-9326/ac5ae2.
Ridder, N.N., Pitman, A.J., Westra, S., Ukkola, A., Do, H.X., Bador, M., Hirsch, A.L., Evans, J.P., di Luca, A., Zscheischler, J., 2020. Global hotspots for the occurrence of compound events. Nat. Commun. 11 (1 11), 1–10. https://doi.org/10.1038/s41467-020-19639-3, 2020.
Ridder, N.N., Pitman, A.J., Ukkola, A.M., 2021. Do CMIP6 climate models simulate global or regional compound events skillfully? Geophys. Res. Lett. 48, e2020GL091152 https://doi.org/10.1029/2020GL091152.
Ridder, N.N., Ukkola, A.M., Pitman, A.J., Perkins-Kirkpatrick, S.E., 2022. Increased occurrence of high impact compound events under climate change. NPJ Clim. Atmos. Sci. 5, 3. https://doi.org/10.1038/s41612-021-00224-4.
Rohde, R., Muller, R., Jacobsen, R., Perlmutter, S., Rosenfeld, A., Wurtele, J., Curry, J., Wickham, C., Mosher, S., 2013. Berkeley Earth temperature averaging process. Geoinf. Geostatistics: An Overv. 1, 1–13.
Saji, N.H., Goswami, B.N., Vinayachandran, P.N., Yamagata, T., 1999. A dipole mode in the tropical Indian ocean. Nature 401, 360–363. https://doi.org/10.1038/43854.
Schaller, N., Sillmann, J., Anstey, J., Fischer, E.M., Grams, C.M., Russo, S., 2018. Influence of blocking on Northern European and Western Russian heatwaves in large climate model ensembles. Environ. Res. Lett. 13, 054015 https://doi.org/10.1088/1748-9326/AABA55.
Seneviratne, S., Nicholls, N., Easterling, D., Goodess, C., Kanae, S., Kossin, J., Luo, Y., Marengo, J., McInnes, K., Rahimi, M., 2012. Changes in climate extremes and their impacts on the natural physical environment. In: Field, C.B., Barros, V., Stocker, T.F., Qin, D., Dokken, D.J., Ebi, K.L., Mastrandrea, M.D., Mach, K.J., Plattner, G.-K., Allen, S.K., Tignor, M., Midgley, P.M. (Eds.), Mloanaging the Risks of Extreme Events and Disasters to Advance Climate Change Adaptation, A Special Report of Working Groups I and II of the Intergovernmental Panel on Climate Change (IPCC). Cambridge University Press, Cambridge, UK, and New York, NY, USA, pp. 109–123.
Sharma, S., Mujumdar, P., 2017. Increasing frequency and spatial extent of concurrent meteorological droughts and heatwaves in India. Sci. Rep. 7 (1 7), 1–9. https://doi.org/10.1038/s41598-017-15896-3, 2017.
Sharples, J.J., Cary, G.J., Fox-Hughes, P., Mooney, S., Evans, J.P., Fletcher, M.S., Fromm, M., Grierson, P.F., McRae, R., Baker, P., 2016. Natural hazards in Australia: extreme bushfire. Climatic Change 139, 85–99. https://doi.org/10.1007/s10584-016-1811-1.
Shi, Z., Jia, G., Zhou, Y., Xu, X., Jiang, Y., 2021. Amplified intensity and duration of heatwaves by concurrent droughts in China. Atmos. Res. 261 https://doi.org/10.1016/j.atmosres.2021.105743.
Singh, J., Ashfaq, M., Skinner, C.B., Anderson, W.B., Singh, D., 2021. Amplified risk of spatially compounding droughts during co-occurrences of modes of natural ocean variability. NPJ Clim. Atmos. Sci. 4, 1–14. https://doi.org/10.1038/s41612-021-00161-2.
Singh, J., Ashfaq, M., Skinner, C.B., Anderson, W.B., Mishra, V., Singh, D., 2022. Enhanced risk of concurrent regional droughts with increased ENSO variability and warming. Nat. Clim. Change 12, 163–170. https://doi.org/10.1038/s41558-021-01276-3.
Spinoni, J., Naumann, G., Carrao, H., Barbosa, P., Vogt, J., 2014. World drought frequency, duration, and severity for 1951–2010. Int. J. Climatol. 34, 2792–2804. https://doi.org/10.1002/JOC.3875.
Suarez-Gutierrez, L., Müller, W.A., Li, C., Marotzke, J., 2020. Hotspots of extreme heat under global warming. Clim. Dynam. 55 (3 55), 429–447. https://doi.org/10.1007/S00382-020-05263-W, 2020.
WMO, Svoboda, M., Hayes, M., Wood, D., 2012. Standardized precipitation index user guide. WMO, Geneva, 1094 (WMO-No. 1090).
Swart, N.C., Cole, J.N.S., Kharin, V.v., Lazare, M., Scinocca, J.F., Gillett, N.P., Anstey, J., Arora, V., Christian, J.R., Hanna, S., Jiao, Y., Lee, W.G., Majaess, F., Saenko, O.A., Seiler, C., Seinen, C., Shao, A., Sigmond, M., Solheim, L., von Salzen, K., Yang, D., Winter, B., 2019. The Canadian Earth system model version 5 (CanESM5.0.3). Geosci. Model Dev. (GMD) 12, 4823–4873. https://doi.org/10.5194/GMD-12-4823-2019.
Trenberth, K.E., 1997. The definition of El Niño. Bull. Am. Meteorol. Soc. 78, 2771–2778.
Ukkola, A.M., Pitman, A.J., Donat, M.G., de Kauwe, M.G., Angélil, O., 2018. Evaluating the contribution of land-atmosphere coupling to heat extremes in CMIP5 models. Geophys. Res. Lett. 45, 9003–9012. https://doi.org/10.1029/2018GL079102.
Ukkola, A.M., de Kauwe, M.G., Roderick, M.L., Abramowitz, G., Pitman, A.J., 2020. Robust future changes in meteorological drought in CMIP6 projections despite uncertainty in precipitation. Geophys. Res. Lett. 47 https://doi.org/10.1029/2020GL087820 e2020GL087820.
Ummenhofer, C.C., England, M.H., McIntosh, P.C., Meyers, G.A., Pook, M.J., Risbey, J.S., Gupta sen, A., Taschetto, A.S., 2009. What causes southeast Australia's worst droughts? Geophys. Res. Lett. 36 https://doi.org/10.1029/2008GL036801.
Ummenhofer, C.C., Gupta sen, A., Briggs, P.R., England, M.H., McIntosh, P.C., Meyers, G. A., Pook, M.J., Raupach, M.R., Risbey, J.S., 2011. Indian and pacific ocean influences on southeast Australian drought and soil moisture. J. Clim. 24, 1313–1336. https://doi.org/10.1175/2010JCLI3475.1.
Vicente-Serrano, S.M., Beguería, S., López-Moreno, J.I., 2010. A multiscalar drought index sensitive to global warming: the standardized precipitation evapotranspiration index. J. Clim. 23, 1696–1718. https://doi.org/10.1175/2009JCLI2909.1.
Vogel, J., Paton, E., Aich, V., Bronstert, A., 2021. Increasing compound warm spells and droughts in the Mediterranean Basin. Weather Clim. Extrem. 32 https://doi.org/10.1016/j.wace.2021.100312.
Voldoire, A., Saint-Martin, D., Sénési, S., Decharme, B., Alias, A., Chevallier, M., Colin, J., Guérémy, J.F., Michou, M., Moine, M.P., Nabat, P., Roehrig, R., Salas y Mélia, D., Séférian, R., Valcke, S., Beau, I., Belamari, S., Berthet, S., Cassou, C., Cattiaux, J., Deshayes, J., Douville, H., Ethé, C., Franchistéguy, L., Geoffroy, O., Lévy, C., Madec, G., Meurdesoif, Y., Msadek, R., Ribes, A., Sanchez-Gomez, E., Terray, L., Waldman, R., 2019. Evaluation of CMIP6 DECK experiments with CNRM-CM6-1. J. Adv. Model. Earth Syst. 11, 2177–2213. https://doi.org/10.1029/2019MS001683.
Wiedermann, M., Siegmund, J.F., Donges, J.F., Donner, R.v., 2021. Differential imprints of distinct ENSO flavors in global patterns of very low and high seasonal precipitation. Frontiers in Climate 3, 5. https://doi.org/10.3389/FCLIM.2021.618548.
Wood, R.R., Lehner, F., Pendergrass, A.G., Schlunegger, S., 2021. Changes in precipitation variability across time scales in multiple global climate model large ensembles. Environ. Res. Lett. 16, 084022 https://doi.org/10.1088/1748-9326/AC10DD.
Wu, X., Hao, Z., Hao, F., Zhang, X., Singh, V.P., Sun, C., 2021. Influence of large-scale circulation patterns on compound dry and hot events in China. J. Geophys. Res. Atmos. 126, e2020JD033918 https://doi.org/10.1029/2020JD033918.
Zscheischler, J., Martius, O., Westra, S., Bevacqua, E., Raymond, C., Horton, R.M., van den Hurk, B., AghaKouchak, A., Jézéquel, A., Mahecha, M.D., Maraun, D., Ramos, A. M., Ridder, N.N., Thiery, W., Vignotto, E., 2020. A typology of compound weather and climate events. Nat. Rev. Earth Environ. 1 (7 1), 333–347. https://doi.org/10.1038/s43017-020-0060-z, 2020.